AMERICAN SOCIETY FOR MICROBIOLOGY | Molecular and Cellular Biology

C/EBPγ Is a Critical Regulator of Cellular Stress Response Networks through Heterodimerization with ATF4

Christopher J. Huggins,[a] Manasi K. Mayekar,[a] Nancy Martin,[a] Karen L. Saylor,[b] Mesfin Gonit,[a] Parthav Jailwala,[c] Manjula Kasoji,[c] Diana C. Haines,[d] Octavio A. Quiñones,[e] Peter F. Johnson[a]

Mouse Cancer Genetics Program, Center for Cancer Research, National Cancer Institute, Frederick, Maryland, USA[a]; Laboratory Animal Sciences Program, Leidos Biomedical Research, Inc., Frederick National Laboratory for Cancer Research, Frederick, Maryland, USA[b]; Advanced Biomedical Computing Center, Leidos Biomedical Research, Inc., Frederick National Laboratory for Cancer Research, Frederick, Maryland, USA[c]; Pathology/Histotechnology Laboratory, Leidos Biomedical Research, Inc., Frederick National Laboratory for Cancer Research, Frederick, Maryland, USA[d]; DMS, Inc., Frederick National Laboratory for Cancer Research, Frederick, Maryland, USA[e]

The integrated stress response (ISR) controls cellular adaptations to nutrient deprivation, redox imbalances, and endoplasmic reticulum (ER) stress. ISR genes are upregulated in stressed cells, primarily by the bZIP transcription factor ATF4 through its recruitment to *cis*-regulatory C/EBP:ATF response elements (CAREs) together with a dimeric partner of uncertain identity. Here, we show that C/EBPγ:ATF4 heterodimers, but not C/EBPβ:ATF4 dimers, are the predominant CARE-binding species in stressed cells. C/EBPγ and ATF4 associate with genomic CAREs in a mutually dependent manner and coregulate many ISR genes. In contrast, the C/EBP family members C/EBPβ and C/EBP homologous protein (CHOP) were largely dispensable for induction of stress genes. *Cebpg*$^{-/-}$ mouse embryonic fibroblasts (MEFs) proliferate poorly and exhibit oxidative stress due to reduced glutathione levels and impaired expression of several glutathione biosynthesis pathway genes. *Cebpg*$^{-/-}$ mice (C57BL/6 background) display reduced body size and microphthalmia, similar to ATF4-null animals. In addition, C/EBPγ-deficient newborns die from atelectasis and respiratory failure, which can be mitigated by *in utero* exposure to the antioxidant *N*-acetylcysteine. *Cebpg*$^{-/-}$ mice on a mixed strain background showed improved viability but, upon aging, developed significantly fewer malignant solid tumors than WT animals. Our findings identify C/EBPγ as a novel antioxidant regulator and an obligatory ATF4 partner that controls redox homeostasis in normal and cancerous cells.

A variety of stresses, such as amino acid limitation, protein misfolding in the endoplasmic reticulum (ER), oxidative stress, hypoxia, and intracellular pathogens, activate gene expression programs collectively known as the integrated stress response (ISR) (1). Stress-induced genes are involved in multiple cellular processes that include nutrient uptake, amino acid synthesis, metabolic changes, antioxidant defenses, and cell survival, leading to cell recovery and alleviation of stress. However, prolonged or irresolvable stress can trigger cell death (2).

Protein misfolding and ER stress are associated with several diseases, including diabetes and neurodegenerative disorders such as amyotrophic lateral sclerosis (ALS), Alzheimer's disease, and Huntington's disease (3). The ISR also plays an important role in cancer as tumor cells frequently experience nutrient deprivation, hypoxia, and oxidative stress and require stress response regulators such as the transcription factor (TF) ATF4 to thrive under adverse conditions (4, 5). Elevated levels of reactive oxygen species (ROS) can initiate oncogenesis by causing DNA mutations and genome instability (6). However, recent studies have shown that, once established, tumor cells are reliant on antioxidant pathways for growth and survival (7, 8). Moreover, radio- and chemotherapies induce death or senescence of cancer cells partly by increasing ROS. Thus, acquiring a detailed understanding of the pathways and mechanisms that regulate stress response genes may lead to improved treatments for cancer and other diseases.

The ISR is initiated by one of several stress kinases, the most common of which is PERK. PERK is activated by ER stress and redox imbalances and constitutes one arm of the unfolded protein response (UPR) (9). Stress kinases phosphorylate eukaryotic translation initiation factor 2α (eIF2α), inhibiting its activity and causing a global reduction in protein synthesis. Paradoxically, these conditions also stimulate translation of certain mRNAs such as ATF4. Upon its expression, ATF4 promotes transcription of many stress-activated genes and is considered the master stress response regulator (10). One of the important targets of ATF4 is C/EBP homologous protein (CHOP), which can promote cell death following acute or unresolved stress (11).

Although ATF4 can bind to ATF/CREB sites as a homodimer or heterodimer with other ATFs, many stress genes contain *cis*-regulatory motifs that recognize heterodimers composed of C/EBP and ATF subunits. These sequences, known as C/EBP:ATF response elements (CAREs) or amino acid response elements (AAREs), consist of one ATF/CREB half-site and one C/EBP half-site (12). In stressed cells, ATF4 or, in some cases, ATF2 or ATF5 is recruited together with a C/EBP subunit to CARE-containing promoters (13). C/EBPβ has been suggested to serve as an ATF4 partner that regulates transcription of certain ISR genes (14, 15) and is capable of heterodimerizing with ATF4 and other ATF family

Received 1 October 2015 **Returned for modification** 30 October 2015
Accepted 7 December 2015

Accepted manuscript posted online 28 December 2015

Citation Huggins CJ, Mayekar MK, Martin N, Saylor KL, Gonit M, Jailwala P, Kasoji M, Haines DC, Quiñones OA, Johnson PF. 2016. C/EBPγ is a critical regulator of cellular stress response networks through heterodimerization with ATF4. Mol Cell Biol 36:693–713. doi:10.1128/MCB.00911-15.

Address correspondence to Peter F. Johnson, johnsope@mail.nih.gov.

C.J.H. and M.K.M contributed equally to this article.

Supplemental material for this article may be found at http://dx.doi.org/10.1128/MCB.00911-15.

members (16, 17). However, cells lacking C/EBPβ remain capable of activating many genes induced by ER stress or amino acid deficiency and, indeed, display increased or prolonged expression of some ATF4 targets (15, 18). Thus, the identity of the C/EBP protein that dimerizes with ATF4 to activate transcription through CARE motifs in stressed cells remains unclear.

C/EBPγ is a small C/EBP family member that harbors a C-terminal bZIP DNA-binding domain but lacks a transactivation domain present in C/EBP activator proteins (19, 20). C/EBPγ cannot form stable homodimers (21) and preferentially heterodimerizes with other C/EBP members, typically inhibiting their transcriptional activities (19, 22). Analysis of *Cebpg*$^{-/-}$ mouse fibroblasts showed that C/EBPγ promotes cell proliferation and suppresses senescence, in part by heterodimerizing with C/EBPβ (23). However, in general the regulatory and biological functions of C/EBPγ are not well characterized. Here, we report that C/EBPγ is a critical regulator of stress-induced genes and binds to CAREs as a heterodimer with ATF4. C/EBPγ-deficient MEFs display oxidative stress resulting from reduced glutathione pools, causing impaired proliferation. *Cebpg*$^{-/-}$ and *Atf4*$^{-/-}$ cells show highly overlapping sets of disregulated target genes, and mice lacking either protein exhibit microphthalmia and growth defects. *Cebpg*$^{-/-}$ animals also die shortly after birth due to impaired lung inflation and respiratory distress, which can be significantly ameliorated by prenatal exposure to the antioxidant *N*-acetylcysteine (NAC). Our data identify C/EBPγ as a critical regulator of cellular stress responses through its role as an ATF partner.

MATERIALS AND METHODS

Animal procedures and preparation of MEFs. C57BL/6 *Cebpg*$^{+/-}$ mice (24) were kindly provided by Tsuneyasu Kaisho; C57BL/6 *Atf4*$^{+/-}$ mice were purchased from Jackson Laboratories (Bar Harbor, ME). Both strains were continuously backcrossed to C57BL/6 mice. Breeding of C57BL/6 *Cebpg*$^{+/-}$ and *Cebpb*$^{+/-}$ mice (25) to generate wild-type (WT) and mutant mouse embryonic fibroblasts (MEFs) was performed as described previously (23, 26). MEFs were prepared from embryonic day 13.5 (E13.5) embryos and cultured in Dulbecco's modified Eagle's medium (DMEM; Invitrogen) supplemented with 10% fetal bovine serum (FBS; Gibco) and 100 U/ml penicillin-streptomycin (Gibco). Crosses to generate WT and *Cebpg*$^{-/-}$ mice on a C57BL/6 × 129Sv hybrid (F1) background were carried out as described previously (23). The National Cancer Institute (NCI)—Frederick is accredited by AAALAC International and follows the Public Health Service Policy for the Care and Use of Laboratory Animals. Animal care was provided in accordance with the procedures outlined in the *Guide for the Care and Use of Laboratory Animals* (27).

NAC supplementation protocol. Mice were mated and monitored for appearance of pregnancy plugs. When pregnancy was determined (approximately days 9 to 11), the mother's water was supplemented with 80 mM *N*-acetylcysteine (NAC) (Santa Cruz Biotechnology), and chow was soaked with 80 mM NAC solution. NAC supplementation was continued until parturition. After birth, pups were fostered to a non-NAC-treated nursing mother and monitored.

Animal pathology evaluation. *Cebpg*- and *Atf4*-positive newborn mice were weighed at birth and genotyped at birth or weaning. E18 (*Cebpg*) and newborn (*Cebpg* and *Atf4*) pups of all genotypes (<24 h to 72 h postpartum) were fixed in 10% neutral buffered formalin (NBF) or Bouin's solution or embedded in optimum cutting temperature (OCT) compound. For the aging study, all adult mice submitted for histopathology analysis underwent a thorough necropsy with tissue fixation in 10% NBF. Fixed pups and select tissues, including any grossly noted abnormalities, in the adult mice were routinely processed to paraffin blocks. Four- to 5-μm-thick sections from the paraffin blocks or 10-μm sections from the OCT blocks were stained with hematoxylin and eosin (H&E) and evaluated by a board-certified veterinary pathologist (D. C. Haines).

Cells and cell culture. MEFs, GP2 packaging cells (provided by S. Hughes), 293T cells (ATCC), and A549 (ATCC) cells were cultured in DMEM supplemented with 10% FBS (Gibco) and maintained at 37°C in 5% CO_2–95% air. NIH 3T3 cells were cultured in DMEM supplemented with 10% FCS (Invitrogen). *Atf4*$^{-/-}$ MEFs were passaged in medium supplemented with 1× nonessential amino acids (NEAA; Sigma) and 55 μM β-mercaptoethanol (Sigma) (1). *Cebpg*$^{-/-}$ MEFs were propagated in medium containing 1 mM NAC. All media were supplemented with 100 U/ml penicillin-streptomycin (Gibco). Stress responses were induced in several ways. ER stress was induced by adding 2 μM thapsigargin (Tg; Sigma). Amino acid deprivation (AAD) was accomplished by one of three methods: (i) cysteine deprivation was achieved by supplementing cysteine-methionine-glutamine-deprived DMEM (Invitrogen) with 1× glutamine (Invitrogen), 1× methionine (Sigma), 1× sodium pyruvate (Invitrogen), and 10% FBS; (ii) glutamine deprivation was achieved by culturing cells in glutamine-deficient medium (Invitrogen) supplemented with 10% FBS; (iii) complete amino acid deprivation was achieved by culturing cells in Krebs-Ringer Buffer (Sigma), 1× sodium pyruvate (Invitrogen), 1× GlutaMAX (Invitrogen), 2 mM His-OH (Sigma), and 5% dialyzed FBS (Invitrogen). Where indicated in the text and figure legends, medium was supplemented with 1 mM NAC, 1 mM GSH (Sigma), or 0.152 mM L-cystine (Sigma).

Plasmids, retroviral vectors, and virus infection. Mouse *Cebpg* and *Atf4* cDNAs were reverse transcribed from WT MEF RNA and ligated into pcDNA3.1 and pBabe-puro vectors. Flag-tagged ATF4 was generated by adding the FLAG epitope sequence to the N terminus of ATF4 during PCR amplification. The sequence of the short hairpin RNA targeting human *CEBPG* (sh*CEBPG*) and retroviral packaging/infection procedures were described previously (23). The mouse *Chop* knockdown lentiviral vector (pLKO.1 puro) was purchased from Sigma-Aldrich (SHCLNG; GenBank accession number NM_007837). Lentiviral vectors, along with envelope and packaging plasmids (pMD2G, Addgene plasmid 12259; pMDLg/RRE, Addgene plasmid 12251; pRSV/Rev, Addgene plasmid 12253), were transfected into HEK293T cells by the calcium phosphate method. At 18 to 20 h after transfection, the medium was changed, and viral supernatants were collected at ~40 h, 47 h, and 63 h posttransfection, filtered through a 0.45-μm-pore-size filter, supplemented with 8 μg/ml Polybrene, and used to infect MEFs. Cells were selected for 3 days in 2 μg/ml puromycin.

Cell proliferation and colony growth assays. Cell proliferation assays of retrovirally infected MEFs (passages 1 to 3) seeded at 2.5×10^4 cells/well in six-well plates (in triplicate) were carried out as previously described (23). All values were normalized to day 0 (1 day after cell plating). Colony assays for WT and *Cebpg*$^{-/-}$ MEFs (2.5×10^4 cells/100-mm plate) incubated under 20% O_2 or reduced oxygen (5% O_2) conditions and for A549 adenocarcinoma cells (500 cells/100-mm plate) were carried out as described previously (23). NAC supplementation of A549 colony assays was performed using 0.5 mM NAC, which was refreshed every 3 days. Colonies were counted after 14 days; assays were carried out in duplicate.

ROS measurement. Dichlorofluorescein (DCF) (Invitrogen) was used to indirectly measure levels of reactive oxygen species in cells. A total of 1×10^6 WT or *Cebpg*$^{-/-}$ MEFs were plated in 150-mm dishes and grown for 48 h. A total of 5×10^5 A549 cells were plated in 100-mm tissue culture plates and grown for 48 to 72 h. Cells were washed two times in phosphate-buffered saline (PBS) and incubated with 1 μM DCF in PBS for 30 min at 37°C. Cells were then washed two times in PBS, trypsinized, and analyzed with a FACSCalibur instrument (Becton Dickinson).

Glutathione assay. WT and *Cebpg*$^{-/-}$ MEFs (1×10^6) were plated in 150-mm dishes with and without NAC supplementation (1 mM) and grown for 48 h. Cells were collected, and measurements of glutathione (GSH) levels were carried out using a glutathione detection kit (Enzo Life Sciences).

SA-β-Gal staining. Control and sh*CEBPG* A549 cells were plated at a density of 2.5×10^4 cells in six-well plates and cultured for 3 to 4 days at 37°C. Cells were fixed and stained for senescence-associated (SA) β-galactosidase (SA-β-Gal) according to the manufacturer's instructions (senescence detection kit; Calbiochem).

Transient transfection. Transient transfections of 293T and NIH 3T3 cells were carried out in 100-mm dishes at 1.6×10^6 cells/plate using XtremeGENE HP (Roche) according to the manufacturer's specifications. Culture medium was changed at 24 h posttransfection, and the cells were harvested at 48 h posttransfection.

Immunoblotting and coimmunoprecipitation. MEF nuclear extracts were prepared as described previously (28). Briefly, cells were washed once with PBS, scraped, resuspended in lysis buffer (20 mM HEPES, pH 7.9, 1 mM EDTA, 10 mM NaCl, 1 mM dithiothreitol [DTT], 0.1% Nonidet P-40, 0.5 mM phenylmethylsulfonyl fluoride) and incubated on ice for 10 min. Nuclei were pelleted by centrifugation at 3,500 rpm for 10 min. Proteins were extracted from nuclei by incubation in high-salt buffer (25 mM HEPES, pH 7.9, 0.2 mM EDTA, 0.42 M NaCl, 0.2 mM DTT, 25% glycerol, 0.5 mM phenylmethylsulfonyl fluoride) at 4°C for 20 min with vigorous shaking. Nuclear debris was pelleted by centrifugation at 14,000 rpm for 5 min, and the supernatant was used for further experiments or stored at −70°C. Nuclear extract (20 to 50 μg) was resolved by 12% to 16% SDS-PAGE and blotted onto nitrocellulose membranes (Millipore). For coimmunoprecipitation experiments, transiently transfected 293T cells were washed twice with cold PBS and lysed using Triton X (Sigma) lysis buffer (50 mM Tris-HCl [pH 7.4], 1% Triton X, 0.1% SDS, 150 mM NaCl, 1 mM EDTA). Lysates were incubated on ice for 10 min, and cell debris was removed by centrifugation at 14,000 rpm at 4°C for 10 min. Protein concentrations were normalized and immunoprecipitated overnight at 4°C with 0.5 μg of FLAG antibody. Protein G (Santa Cruz) beads were added to overnight precipitations for 2 h. Beads were washed three times in lysis buffer and resuspended in 5× SDS loading dye. Proteins were resolved by 12% SDS-PAGE and blotted onto nitrocellulose membranes. Protein concentrations were determined using a Bradford protein assay (Bio-Rad). All buffers described above were supplemented with phosphatase and protease inhibitors (Calbiochem). Primary antibodies used were as follows: FLAG (M2) (Sigma); NRF2 (C-20), actin (H-196), C/EBPβ (C-19), and ATF4 (C-20) (Santa Cruz Biotechnologies); MEK1 (9124) and MEK2 (9125) (Cell Signaling Technologies); and C/EBPγ C-terminal antibody (22). Secondary antibodies conjugated to horseradish peroxidase (Promega) were used to detect antigen-antibody complexes by a chemiluminescent ECL detection system (Pierce).

EMSA. Electrophoretic mobility shift assays (EMSAs) were performed as described previously (22). EMSA probe sequences are shown in the supplemental data and include core CARE sequences from *Snat2* and *Asns* (TGATGCAAT and TGATGAAAC, respectively) (12) and CARE sites containing flanking genomic sequences for *Asns* (nucleotides [nt] −79 to −53) and *Eif4ebp1*. The consensus C/EBP probe has been described previously (22). Probes were end labeled using [^{32}P]dATP (Amersham) and polynucleotidylkinase (Roche). DNA-binding assays were carried out in 25-μl reaction mixtures containing 20 mM HEPES (pH 7.9), 200 mM NaCl, 5% Ficoll, 1 mM EDTA, 50 mM DTT, 0.01% Nonidet P-40, 1.75 μg of poly(dI-dC), and 2×10^4 cpm probe. After incubation for 20 min at room temperature, 10 to 15 μl of the binding reaction mixture was loaded onto a 6% polyacrylamide gel in Tris-borate-EDTA (TBE; 90 mM Tris base, 90 mM boric acid, 0.5 mM EDTA) buffer and electrophoresed at 160 V for 2 h. Antibody supershift assays were carried out by preincubating the nuclear extract with 1 μl of appropriate antibody at 4°C for 30 min prior to addition of the binding reaction mixture.

Microarray gene expression profiling. RNA for genome-wide transcriptional profiling experiments was isolated from WT, *Cebpg*$^{-/-}$, and *Atf4*$^{-/-}$ MEFs, as described previously (23). A total of 10^6 cells were plated in 150-mm dishes in DMEM–10% FBS with no additional supplementation. Medium was refreshed 24 h later and again at 48 h with either DMEM or AAD medium for 3 h, after which cells were harvested for RNA preparation. Microarray hybridization was carried out using Affymetrix Mouse 430A GeneChips; three biological replicates were analyzed for each MEF population. A set of reference genes that were induced by AAD by ≥1.3-fold in WT MEFs ($P < 0.05$) was first identified. AAD-induced genes that were underexpressed in *Cebpg*$^{-/-}$ or *Atf4*$^{-/-}$ MEFs subjected to AAD were then determined [i.e., fold difference of AAD-induced genes in *Cebpg*$^{-/-}$ or *ATF4*$^{-/-}$ MEFs under amino acid deprivation conditions compared to results for similarly treated WT MEFs ≤−1.3; $P < 0.05$] to identify C/EBPγ-regulated and ATF4-regulated genes, respectively. These gene sets were compared to genes identified through chromatin immunoprecipitation with high-throughput sequencing (ChIP-Seq) analysis as having C/EBPγ and/or ATF4 bound at transcription start site (TSS)-proximal regions (kb −5 to +2) to determine AAD-induced genes that are directly regulated by C/EBPγ and/or ATF4.

Reverse transcription-quantitative PCR (RT-qPCR). RNA isolated from MEF cultures was used to verify expression levels of selected genes. cDNA was generated (reverse transcription kit; Qiagen) from total RNA, and qPCR was performed using SYBR green with QuantiTect Primers (Qiagen) or Primer-PCR Primers (Bio-Rad) and normalized against β-*actin* or *Pp1a*. qPCR analysis was performed using a Bio-Rad CFX96 Touch thermal cycler. In general, relative gene expression values were determined from two biological replicates (assayed in technical triplicates) and the data were averaged. Error bars represent standard errors of the means (SEM) of expression levels.

Statistical analysis. Detailed analysis of microarray gene expression data was carried out as previously described (29). Student's *t* test was used to calculate the statistical significance for RT-qPCR (CFX Manager, version 3.1; Bio-Rad) and ChIP-qPCR data (GraphPad Prism, version 6). The chi-square test and Mantel-Cox log rank test (GraphPad Prism, version 6) were used for calculating the significance of differences between groups in the tumor incidence/mortality data and Kaplan-Meier survival curves, respectively. Comparisons showing a *P* value of ≤0.05 were taken as significantly different.

Chromatin immunoprecipitation. ChIP assays were performed as described previously (23). Briefly, MEFs (one 15-cm dish/ChIP assay) were cross-linked with 1% formaldehyde for 10 min at room temperature, and the reaction was quenched by the addition of 0.125 M glycine. Cells were washed with PBS, resuspended in lysis buffer (0.1% SDS, 0.5% Triton X-100, 150 mM NaCl, 20 mM Tris-HCl, pH 8.1), and sonicated to obtain DNA fragments of ~500 bp. The cleared sonicate was diluted 1:5 with ChIP dilution buffer (0.01% SDS, 1.1% Triton X-100, 1.2 mM EDTA, 167 mM NaCl). Immunoprecipitation was performed using the following antibodies: 5 μg of anti-green fluorescent protein (anti-GFP) (FL; Santa Cruz Biotechnologies), anti-ATF4 (C-20; Santa Cruz Biotechnologies) for ChIP-Seq, a polyclonal ATF4 antibody kindly provided by M. Kilberg (30) for ChIP-qPCR, or anti-C/EBPγ C-terminal antiserum (22) with overnight rotation at 4°C. Protein A magnetic beads (New England BioLabs) were used for immunoprecipitation; precipitates were washed twice each with low-salt buffer, high-salt buffer, LiCl immune complex buffer, and 1× Tris-EDTA (TE) buffer and processed for DNA purification. All lysis and wash buffers were supplemented with Complete Mini protease inhibitor cocktail tablets (Roche). DNA was isolated using a Wizard SV gel and PCR Clean-Up system (Promega), and DNA was amplified by qPCR (Bio-Rad CFX96); PCR primers are listed in the supplemental data. ChIP-Seq methods and data analysis are described in the supplemental data.

Bioinformatics. Initial pathway analysis of *Cebpg*$^{-/-}$ versus WT MEF differential gene expression was performed using GeneGo tools (MetaCore) with criteria of a >2-fold increase/decrease and a *P* value of <0.001. We also used Ingenuity Pathway Analysis (IPA; Qiagen) to analyze gene expression differences and ChIP-Seq data.

Lipidomics analysis. Lungs from newborn mice were homogenized in PBS using a motorized pestle. Total lipids were extracted from the homogenate by adding 2 ml of chloroform and 4 ml of methanol to 1.6 ml of the

aqueous homogenate, shaking well, and then adding 2 ml of chloroform and 2 ml of water. Two additional extractions were performed with 2 ml of chloroform. Butylated hydroxytoluene (0.01%) was added to the chloroform used for all the extractions. All the organic phases were combined, washed once with 0.5 ml of 1 M potassium chloride and once with 0.5 ml of water, dried in a nitrogen evaporator, and then stored at −80°C. Samples were analyzed by mass spectrometry at the Kansas Lipidomics Research Center, Kansas State University. The primary lipidomics data are included in Table S5 in the supplemental material.

Microarray data accession numbers. Microarray data were deposited in the Gene Expression Omnibus (GEO) database under accession number GSE75150, and ChIP-Seq data were deposited under accession number GSE75165.

RESULTS

C/EBPγ-deficient cells display oxidative stress due to impaired glutathione synthesis. MEFs lacking C/EBPγ proliferate poorly and exhibit increased senescence relative to levels in WT cells (23) (Fig. 1A). To explore the molecular basis for defective proliferation/survival of the mutant cells, we analyzed microarray gene expression data from WT and *Cebpg*$^{-/-}$ cells (±2-fold expression difference; *P* value of <0.001) (23). GeneGo analysis identified two pathways that may contribute to the mutant phenotype: (i) the role of Akt in hypoxia-induced HIF1 activation and (ii) the role of ASK1 under oxidative stress (Fig. 1B). These observations suggest that *Cebpg*$^{-/-}$ MEFs are experiencing oxidative stress, causing impaired cell growth/survival. Accordingly, the mutant cells displayed a 4-fold increase in ROS levels (Fig. 1C), elevated nuclear expression of the oxidative stress regulator Nrf2 (Fig. 1D), and upregulation of several oxidative stress response genes (Fig. 1E). These include *Hmox1* and *Nqo1* (Fig. 1F), whose expression returned to basal levels when the cells were treated with the antioxidant NAC. In addition, colony assays of *Cebpg*$^{-/-}$ MEFs cultured under normal-oxygen (20%) or low-oxygen (5%) conditions showed significantly increased clonogenic growth under reduced O_2 (Fig. 1G), further supporting an impairment in the cells' ability to alleviate oxidative stress. Addition of NAC effectively restored proliferation of *Cebpg*$^{-/-}$ MEFs, which grew comparably to WT cells (Fig. 1H, upper panel, and I); NAC also caused a dramatic normalization of cellular morphology (Fig. 1H, lower panel). These findings show that loss of C/EBPγ leads to elevated ROS and impaired cell proliferation/survival.

We next compared the gene signatures of *Cebpg*$^{-/-}$ and WT MEFs to identify metabolic pathways that might be disregulated in the mutant cells, thus causing oxidative stress (Fig. 2A). Two of the most significantly affected pathways were glutathione metabolism (Fig. 2A, pathway 1) and ROS metabolism (pathway 5). The reduced form of glutathione (GSH), a cysteine-containing tripeptide, is the most abundant intracellular antioxidant. GSH levels in *Cebpg*$^{-/-}$ MEFs were significantly diminished compared to levels in WT cells (Fig. 2B), and the ratio of reduced to oxidized glutathione was also modestly decreased (data not shown). NAC treatment restored glutathione levels, presumably through the ability of NAC to replenish intracellular cysteine (Fig. 2B). In addition, adding glutathione to the culture medium rescued proliferation of the mutant cells while addition of cystine (oxidized cysteine) partially restored growth (Fig. 2C). These findings indicate that compromised cysteine availability in C/EBPγ-deficient cells leads to impaired GSH synthesis and the inability to neutralize ROS.

Examination of the GSH metabolic pathway (microarray data) showed that several genes are downregulated in *Cebpg*$^{-/-}$ MEFs. One of these is *Cth* (cystathionine γ-lyase), which converts cystathionine to cysteine, a rate-limiting step in cysteine biosynthesis that is critical for GSH production. *Slc7a11* (*xCT*), a component of the cystine/glutamate transporter complex required for cystine import, was also downregulated in *Cebpg*$^{-/-}$ cells. qPCR analysis confirmed decreased expression in *Cebpg*$^{-/-}$ MEFs of these two genes and four others involved in maintaining intracellular GSH levels (*Gpx7*, for glutathione peroxidase 7; *Mthfd2*, for methylenetetrahydrofolate dehydrogenase 2; *Slc1a5*, for a transporter of neutral amino acids such as glutamine; and *Gpt2*, for glutamic pyruvate transaminase) (Fig. 2D). Thus, C/EBPγ directly or indirectly regulates the transcription of genes associated with cysteine biosynthesis/import, GSH synthesis, and glutathione-mediated detoxification of ROS (Fig. 2E).

Stress-induced C/EBPγ:ATF4 heterodimers bind to CARE/AARE sites. Since ATF4 has a critical role in activating gene transcription in response to increased ROS and other stresses though binding to CARE/AARE sites, we asked whether C/EBPγ might be a component of the ATF4 complex that recognizes these sites. Using an EMSA, we examined DNA-protein complexes formed with a canonical CARE probe and nuclear extracts from WT or *Cebpg*$^{-/-}$ MEFs cultured in complete medium or in one lacking glutamine or cysteine to induce stress. As shown in Fig. 3A (lanes 1 to 6), Gln or Cys deprivation induced a CARE-binding species in WT cells that was completely absent in *Cebpg*$^{-/-}$ MEFs. Antibody supershift assays (Fig. 3A, lanes 7 to 12) demonstrated the presence of C/EBPγ and ATF4 but not C/EBPβ in the induced complex (Fig. 3B, lanes 1 to 4). Similar results were obtained using cells treated with thapsigargin (Tg) to induce ER stress (Fig. 3C). Moreover, a canonical C/EBP site probe produced a different set of EMSA complexes composed mainly of C/EBPβ and C/EBPγ (23) but not ATF4 (Fig. 3B, lanes 5 to 8), showing that the C/EBPγ:ATF4 complex binds selectively to CARE sites.

These results were further corroborated by analyzing extracts from WT, *Atf4*$^{-/-}$, and *Cebpb*$^{-/-}$ cells. Amino acid deprivation (AAD) of WT MEFs induced a complex that formed with a probe containing the naturally occurring CARE motif in the *Asns* (asparagine synthetase) promoter (Fig. 3D). This complex was absent in *Cebpg*$^{-/-}$ and *Atf4*$^{-/-}$ cells but was unaffected by loss of C/EBPβ. A known CARE site from the *Eif4ebp1* gene similarly bound C/EBPγ:ATF4 heterodimers (Fig. 3E). Finally, human HepG2 hepatocarcinoma cells deprived of cysteine also induced a CARE-binding species composed of C/EBPγ and ATF4 subunits (Fig. 3F).

Induction of the ATF4 protein by stress signals was comparable in WT and *Cebpg*$^{-/-}$ MEFs (Fig. 3G), showing that the absence of a CARE-binding complex in C/EBPγ-deficient cells is not due to decreased ATF4 expression. Furthermore, C/EBPγ protein levels were increased by AAD stress in WT cells (Fig. 3H). Coimmunoprecipitation assays demonstrated that overexpressed ATF4 and C/EBPγ proteins physically interact independently of stress signals (Fig. 3I). Collectively, these observations demonstrate that a heterodimer composed of ATF4 and C/EBPγ but not C/EBPβ is the major stress-activated CARE-binding species in mouse and human cells.

To address the apparent preferential ability of C/EBPγ (relative to C/EBPβ) to dimerize with ATF4, we compared interhelical interactions in the leucine zipper interfaces of C/EBPγ:ATF4 and C/EBPβ:ATF4 heterodimers. Electrostatic interactions between residues in the g and e positions of leucine zipper helices govern

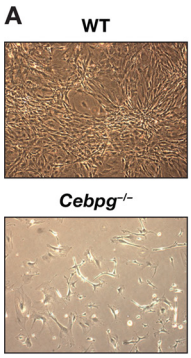

B

	Pathway	p-Value
1	Transcription_Role of Akt in hypoxia induced HIF1 activation	0.000142
2	Cell adhesion_ECM remodeling	0.000167
3	Immune response_Oncostatin M signaling via MAPK in mouse cells	0.000400
4	Immune response_Oncostatin M signaling via MAPK in human cells	0.000496
5	Development_Hedgehog and PTH signaling pathways in bone and cartilage development	0.000496
6	PGE2 pathways in cancer	0.002235
7	Immune response_IL-17 signaling pathways	0.003076
8	Oxidative stress_Role of ASK1 under oxidative stress	0.004751
9	G-protein signaling_RhoA regulation pathway	0.004751
10	G-protein signaling_Regulation of RAC1 activity	0.005588

2-Fold Increase/Decrease, $p \leq 0.001$

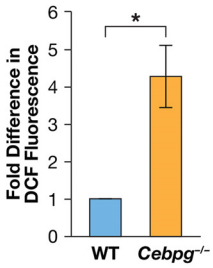

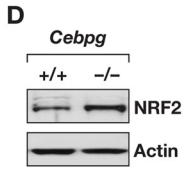

E

Gene	Fold Change	p-Value
Hmox1 [Heme Oxygenase 1]	+6.52	2.06×10^{-6}
Glrx1 [Glutaredoxin 1]	+2.76	5.86×10^{-5}
Hsp72 [Heat Shock Protein 1A]	+4.2	1.18×10^{-5}
Mt2 [Metallothionein 2]	+5.57	2.71×10^{-6}
Nqo2 [NAD(P)H Dehydrogenase, Quinone 1]	+2.34	5.42×10^{-4}
Gsta4 [Glutathione S-Transferase Alpha-4]	+2.71	8.37×10^{-5}
Gclm [Glutamate-Cysteine Ligase, Modifier Subunit]	+2.18	3.92×10^{-5}

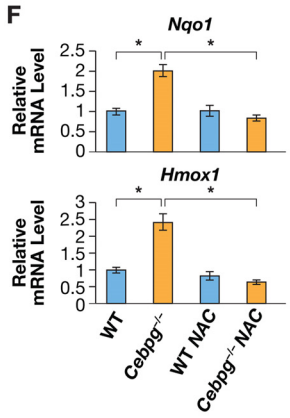

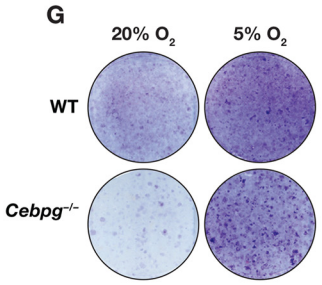

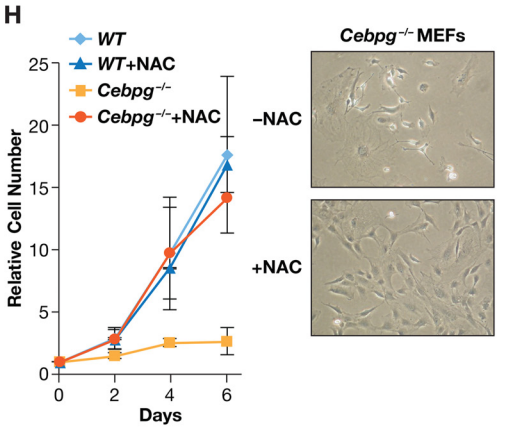

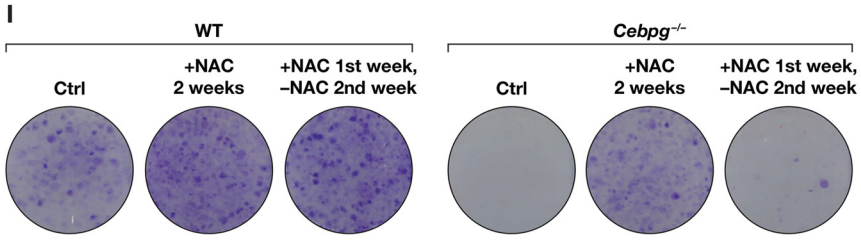

FIG 1 C/EBPγ is required to maintain oxidative homeostasis in MEFs. (A) Morphologies of WT and *Cebpg*$^{-/-}$ MEFs, 48 h after plating. (B) The 10 most significantly affected molecular pathways in *Cebpg*$^{-/-}$ MEFs. Differentially expressed genes from microarray experiments (>2-fold increase/decrease in *Cebpg*$^{-/-}$ versus WT cells; $P \leq 0.01$) were analyzed using GeneGo. (C) Reactive oxygen species (ROS) levels were determined by DCF fluorescence in WT and *Cebpg*$^{-/-}$ MEFs. Data are presented as means ± SEM ($n = 3$). (D) Immunoblot analysis of nuclear NRF2 protein levels in WT and *Cebpg*$^{-/-}$ MEFs. (E) Elevated expression of oxidative stress-induced genes in *Cebpg*$^{-/-}$ MEFs versus WT cells (microarray data). (F) *Hmox1* and *Nqo1* mRNA levels in WT and *Cebpg*$^{-/-}$ MEFs, grown in the absence or presence of NAC. Data are presented as means ± SEM. (G) Colony growth of WT and *Cebpg*$^{-/-}$ MEFs under normal- and low-oxygen conditions. Colonies were visualized 2 weeks after plating. The experiment is a representative example from three replicates. (H) Proliferation of WT and *Cebpg*$^{-/-}$ MEFs cultured in the absence and presence of *N*-acetylcysteine (NAC; 1 mM). Data are presented as means ± standard deviations ($n = 2$). (Right) Micrographs of *Cebpg*$^{-/-}$ MEFs with and without NAC supplementation. (I) Colony growth assays of WT and *Cebpg*$^{-/-}$ MEFs cultured in the absence and presence of 1 mM NAC. Cells were left untreated (−NAC), treated for 2 weeks with NAC (+NAC), or exposed to NAC for 1 week followed by removal for 1 week (−NAC 1 week). *, $P \leq 0.05$.

A

	Pathway Studio: Metabolic	*p*-Value
1	Glutathione metabolism	5.36E-08
2	Mevalonate pathway	1.53E-05
3	Amino sugars synthesis	0.000103702
4	Biosynthesis of cholesterol	0.000111056
5	ROS metabolism	0.000245435
6	Branched chain amino acids metabolism	0.00024693
7	Purine metabolism	0.000439665
8	Fatty acid oxidation	0.00500023
9	Pyrimidine metabolism	0.00563662
10	Metabolism of glycerophospholipids and ether lipids	0.00814873
11	Folate biosynthesis	0.00964123

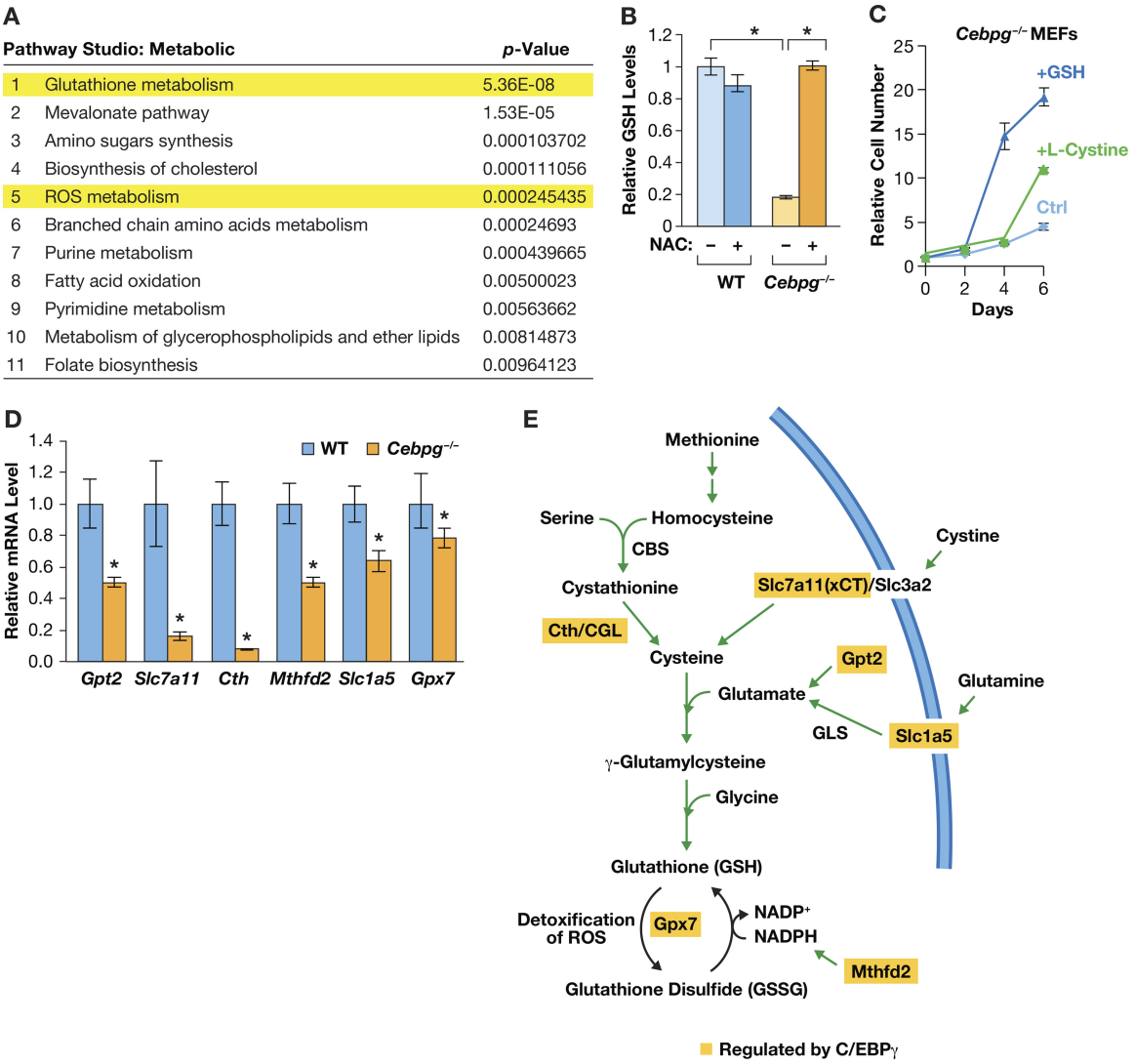

FIG 2 Disregulation of glutathione biosynthesis in cells lacking C/EBPγ. (A) Metabolic pathway analysis (Pathway Studio) of differentially expressed genes in *Cebpg*$^{-/-}$ versus WT MEFs. (B) Glutathione (GSH) levels in WT and *Cebpg*$^{-/-}$ MEFs grown in the absence and presence of NAC (1 mM). (C) Effects of GSH (1 mM) or L-cystine (0.15 mM) on proliferation of WT and *Cebpg*$^{-/-}$ MEFs. Each time point was assayed in triplicate; data are represented as means ± standard deviations. (D) qPCR analysis of genes involved in GSH biosynthesis. (E) C/EBPγ regulates key steps in cysteine biosynthesis/import to generate GSH and alleviate oxidative stress. Cth/CGL, cystathionine γ lyase; Slc7a11 (xCT), solute carrier family 7 (anionic amino acid transporter light chain, Xc-system), member 11; Gpt2, glutamate pyruvate transaminase; Slc1a5, solute carrier family 1 (neutral amino acid transporter, member 5); Gpx7, glutathione peroxidase 7; Mthfd2, NAD-dependent methylenetetrahydrofolate dehydrogenase cyclohydrolase; CBS, cystathionine-beta-synthase; GLS, glutaminase. GSH levels and qPCR data are presented as mean values ± SEM ($n = 2$). *, $P \leq 0.05$.

the specificity and stability of bZIP protein dimerization (31). Enumeration of net attractive and repulsive g↔e′ pairs in the α-helical interfaces shows that C/EBPγ:ATF4 dimers contain six positive g↔e′ interactions, while the C/EBPβ:ATF4 pair forms only four (Fig. 3J). The predicted greater stability of C/EBPγ:ATF4 heterodimers likely accounts for the selective formation of these dimers in stressed cells.

C/EBPγ and ATF4 coregulate many stress-induced genes and associate with common genomic CARE sites. To determine whether C/EBPγ and ATF4 regulate common transcriptional targets, we performed genome-wide profiling of mRNAs induced by amino acid deprivation (AAD) in MEFs. Microarray analysis of RNA from WT, *Cebpg*$^{-/-}$, and *Atf4*$^{-/-}$ MEFs harvested before and after AAD identified 1,566 stress-induced genes in WT cells (thresholds of ≥1.3-fold increase and a *P* value of <0.05) (Fig. 4A). Of these induced genes, 322 (21%) were C/EBPγ dependent, 691 (44%) were ATF4 dependent, and 248 (16%) required both transcription factors. Thus, there is a considerable overlap between the AAD-induced genes regulated by C/EBPγ and by ATF4. These data support an important role for C/EBPγ, together with ATF4, in regulating cellular antioxidant and stress response pathways.

To identify genes directly regulated by C/EBPγ and ATF4 and to investigate their genome-wide association with CAREs, we performed ChIP-Seq analysis of MEFs after AAD induction (Fig. 4; see Fig. S1 in the supplemental material). A total of 2,642 ATF4 and 25,419 C/EBPγ peaks were identified, of which 233 ATF4 (9%) and 2,060 C/EBPγ (8%) peaks were located proximal to

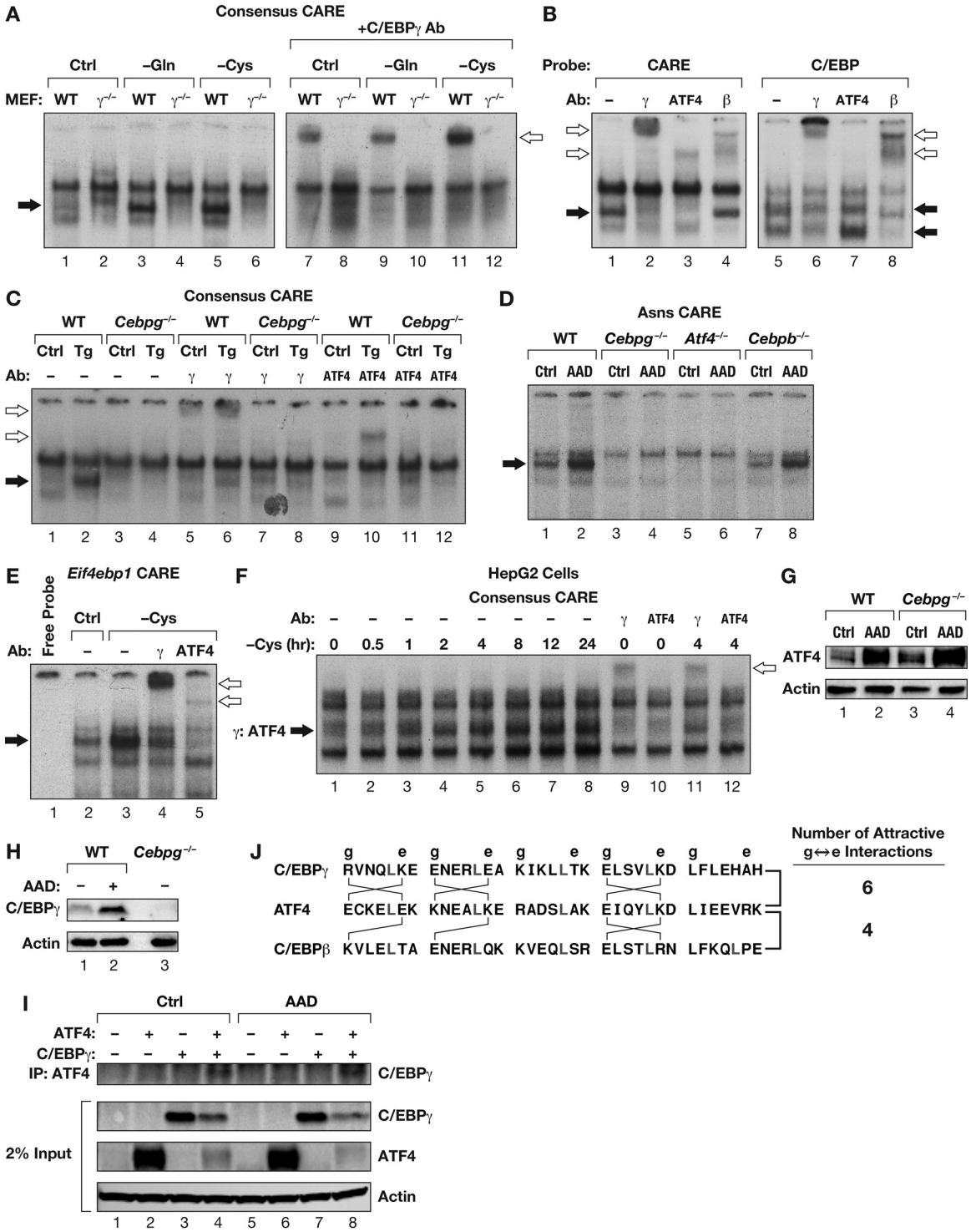

FIG 3 C/EBPγ and ATF4 form heterodimers that bind to CARE/AARE sites. (A) A C/EBPγ DNA-binding species induced by amino acid deprivation binds to a consensus CARE probe. Nuclear extracts from WT and *Cebpg*$^{-/-}$ MEFs cultured in complete medium or medium lacking Gln or Cys (3 h) were analyzed by EMSA using a radiolabeled consensus CARE probe. The presence of C/EBPγ in the induced complex (WT cells) was confirmed by antibody supershifts (lanes 7 to 12). The filled arrow indicates the induced complex; the open arrow indicates supershifted species. The gel was cropped to show only the region containing DNA-protein complexes. (B) The stress-induced CARE-binding species contains C/EBPγ and ATF4 but not C/EBPβ. A nuclear extract from amino acid-deprived WT MEFs was analyzed by EMSA using the CARE probe in the absence and presence of antibodies for C/EBPγ, ATF4, or C/EBPβ (lanes 1 to 4). The assay was repeated using a consensus C/EBP site probe (lanes 5 to 8). (C) Nuclear extracts prepared from WT and *Cebpg*$^{-/-}$ MEFs, untreated or exposed to thapsigargin (Tg; 2 μg/ml for 3 h) to induce ER stress, were analyzed by EMSA using a consensus CARE probe. Supershift assays were used to evaluate the presence of C/EBPγ (lanes 5 to 8) and ATF4 (lanes 9 to 12) in the induced complex. (D) Nuclear extracts from *Cebpg*$^{-/-}$, *Atf4*$^{-/-}$, or *Cebpb*$^{-/-}$ MEFs cultured under normal or amino acid deprivation (AAD) conditions were analyzed by EMSA using a native CARE site probe from the asparagine synthetase gene (*Asns*). (E) A CARE element from the *Eif4ebp1* gene binds a stress-induced complex containing C/EBPγ and ATF4. Nuclear extracts from control or cysteine-deprived

transcription start sites (TSS proximal; kb −5 to +2) (Fig. 4B). This represents enrichment levels of 4.9-fold (ATF4) and 4.5-fold (C/EBPγ) over the binding density predicted from random association across the genome and is comparable to the promoter enrichment reported for ATF4 binding following ER stress (32). A comparison of the ATF4 and C/EBPγ TSS-proximal peaks revealed 83 overlapping (cobound) peaks, corresponding to 80 unique genes (Fig. 4B and C). Distance-to-TSS plots of the peaks revealed a pronounced clustering of C/EBPγ binding events adjacent to TSSs, which was also observed for ATF4 peaks and C/EBPγ-ATF4 cobound peaks (Fig. 4D). Thus, ATF4 and C/EBPγ binding is concentrated in regions around TSSs, consistent with the promoter-proximal locations of functional CARE/AARE sites characterized in many stress genes (13).

We next analyzed the ATF4 and C/EBPγ peaks for the presence of CARE motifs (TGATGNAAN) (Fig. 4E). Approximately 15% of genome-wide ATF4 and C/EBPγ peaks contained CAREs, and this fraction increased to 32% and 23%, respectively, for TSS-proximal peaks. *De novo* motif analysis using sequences from the TSS-proximal peaks showed that the 83 cobound sites generated a motif (TTGCATCA) that is identical to the consensus CARE, and the 233 ATF4-bound sequences identified a similar motif (Fig. 4F). The C/EBPγ-bound sequences produced a low-complexity motif without obvious homology to C/EBP sites (data not shown), possibly because C/EBPγ forms multiple heterodimers that collectively recognize a variety of sequences.

Ingenuity Pathway Analysis (IPA) of the 80 cobound genes revealed tRNA charging as the most significant association, with folate metabolism and amino acid synthesis pathways also displaying high significance (Fig. 4G). These findings corroborate a recent study identifying protein synthesis genes such as tRNA synthetases as a major class of ATF4 targets during ER stress (32). Several tRNA synthetase genes contain CAREs in their promoters that were cobound by ATF4 and C/EBPγ (see Table S1 in the supplemental material). Moreover, folate is known to be a free radical scavenger that displays antioxidant properties (33, 34). Cross-comparison of the ATF4 and C/EBPγ peaks with the 248 common stress-induced genes revealed an intersection of 15 genes that are coregulated and cobound by ATF4 and C/EBPγ (Fig. 4C and Table 1). This is presumably an underestimate of genes fulfilling these criteria, as we used stringent statistical cutoffs and a conservative definition of TSS-proximal regulatory regions for our analysis. As expected, most of the 15 genes are associated with stress responses (e.g., *Trb3*, *Aars*, *Ddit4*/*Redd*, and *Herpud1*) and/or have antioxidant functions (*Sesn2*, *Slc7a11*, and *Gpt2*) (Table 1). Another class of genes is involved in fatty acid and cholesterol metabolism/transport (*Soat2* and *Vldlr*), which may be related to observations linking amino acid deprivation-induced proteotoxic stress with increased ER biogenesis and upregulation of lipogenic pathways (35).

To verify these results, we analyzed AAD-induced expression of several coregulated, cobound genes and other known CARE-regulated genes in WT and mutant MEFs. Each gene was induced by stress in WT MEFs but showed significantly less expression in *Cebpg*$^{-/-}$ and *Atf4*$^{-/-}$ cells (Fig. 5). Additionally, quantitative ChIP assays were performed for a subset of these genes using primers spanning cobound CARE regions (Fig. 6; see also Table S2 in the supplemental material). These data confirmed that both C/EBPγ and ATF4 interact with CAREs in stressed cells. Notably, AAD-induced binding of C/EBPγ to CAREs was virtually absent in *Atf4*$^{-/-}$ cells, and ATF4 binding was similarly disrupted in *Cebpg*$^{-/-}$ MEFs (Fig. 6). Thus, C/EBPγ and ATF4 associate with genomic CAREs in a mutually dependent manner, supporting the notion that they act as a heterodimer.

Cebpg mRNA levels were modestly increased by stress in WT MEFs but not in ATF4-deficient cells (Fig. 7A), raising the possibility that impaired C/EBPγ binding to CAREs in *Atf4*$^{-/-}$ cells is partly a consequence of lower C/EBPγ levels. However, when C/EBPγ was overexpressed in *Atf4*$^{-/-}$ MEFs, it still did not undergo stress-induced binding to the CARE regions of *Asns*, *Slc7a11*, and *Trb3* (Fig. 7B and C). These data confirm that ATF4 is absolutely necessary for C/EBPγ to associate with CARE sites.

Induction of ATF4 target genes requires C/EBPγ but is largely independent of C/EBPβ and CHOP. We next evaluated the relative contributions of various C/EBP family members to the expression of stress response genes. We performed a time course analysis of several ATF4 target genes (*Asns*, *Slc7a11*, *Trb3*, *Cth*, *Mthfd2*, and *Atf5*) after amino acid deprivation in MEFs lacking C/EBPγ, C/EBPβ, or ATF4 or depleted for CHOP using shRNA (Fig. 8). None of the genes was induced in *Atf4*$^{-/-}$ cells. Of the C/EBP family members, C/EBPγ loss decreased expression of all six ATF4-regulated genes, while cells lacking C/EBPβ showed reduced *Atf5* induction; but other stress genes were generally unaffected or actually increased in *Cebpb*$^{-/-}$ MEFs. Ablation of CHOP reduced *Trb3* expression but did not impair expression of the other genes tested and even enhanced the induction of *Cth* and *Mthfd2*. These experiments indicate that C/EBPγ has a uniquely important role relative to the roles of other C/EBP family members in activating transcription of stress response genes.

***Cebpg*$^{-/-}$ mice display atelectasis, respiratory failure, and perinatal mortality that can be suppressed by *in utero* exposure to NAC.** We next addressed whether *Cebpg*$^{-/-}$ mice might display phenotypes that arise from loss of antioxidant and stress response functions of C/EBPγ. Kaisho et al. (24) reported that *Cebpg*$^{-/-}$ mice on a C57BL/6 background exhibit perinatal lethality, with only 11% of mutant neonates surviving beyond 60 h. We observed similar perinatal mortality, with all *Cebpg*$^{-/-}$ pups dying by 48 h; the mutant mice were also mildly runted, weighing ~10% less than WT littermates at birth (Fig. 9A). Notably, newborn *Cebpg*$^{-/-}$ pups showed labored breathing and failed to suckle.

MEFs were used in EMSAs, without or with C/EBPγ or ATF4 antibodies. (F) A CARE-binding complex containing C/EBPγ and ATF4 is induced by Cys deprivation in human HepG2 cells. Supershift assays (lanes 9 to 12) demonstrate the presence of C/EBPγ and ATF4 in the induced complex (indicated by the solid arrow). (G) ATF4 induction is unaffected by the absence of C/EBPγ. WT and *Cebpg*$^{-/-}$ MEFs were subjected to AAD and analyzed by immunoblotting for ATF4 levels. (H) Analysis of C/EBPγ protein levels in nuclear extracts from WT MEFs, without or with AAD treatment (8 h). *Cebpg*$^{-/-}$ MEFs (lane 3) were included as a negative control. (I) C/EBPγ and ATF4 interact in the absence of DNA. 293T cells were transfected with C/EBPγ and/or Flag-ATF4 plasmids; lysates were prepared from control cells or after 3 h of Cys deprivation, immunoprecipitated with Flag antibody, and analyzed by C/EBPγ immunoblotting. Overexpression of each protein decreased the level of the other, for unknown reasons (lanes 4 and 8). (J) C/EBPγ:ATF4 dimers are predicted to be more stable than C/EBPγ:ATF4 dimers. The figure shows aligned leucine zipper sequences (human homologs) indicating attractive g↔e′ interhelical electrostatic interactions for each dimer pair (31). The repeating leucines are shown in red; g and e positions within the leucine zipper helices are indicated. C/EBPγ:ATF4 dimers make six positive g↔e′ interactions, while C/EBPβ:ATF4 has four.

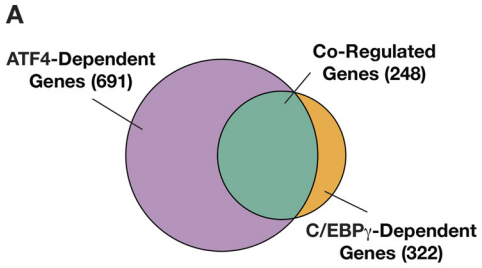

B

	Total Peaks	TSS Proximal Peaks	% TSS Proximal Peaks
ATF4	2642	233	9%
C/EBPγ	25419	2060	8%
ATF4+C/EBPγ	391	83	21%

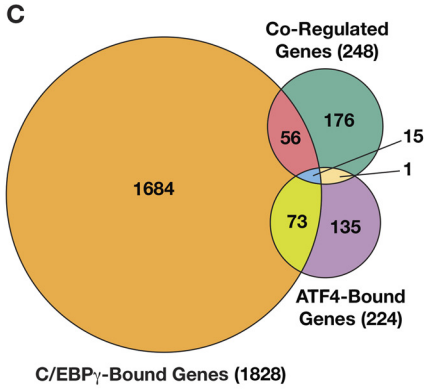

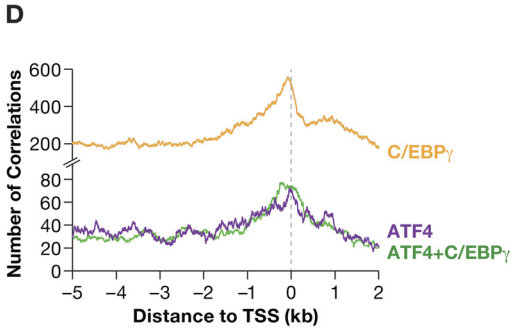

E

	Total Peaks	No. CARE-Containing Peaks (No. of Matches)	% CARE-Containing Peaks	No. TSS-Proximal Peaks	No. CARE-Containing TSS-Proximal Peaks (No. of Matches)	% TSS-Proximal CARE-Containing Peaks
ATF4	2642	391 (451)	14.7%	233	74 (88)	31.7%
C/EBPγ	25419	4033 (4486)	15.8%	2060	472 (526)	22.9%

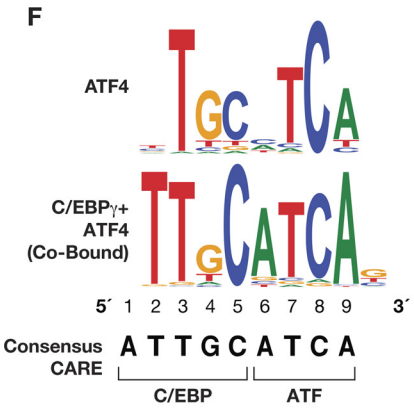

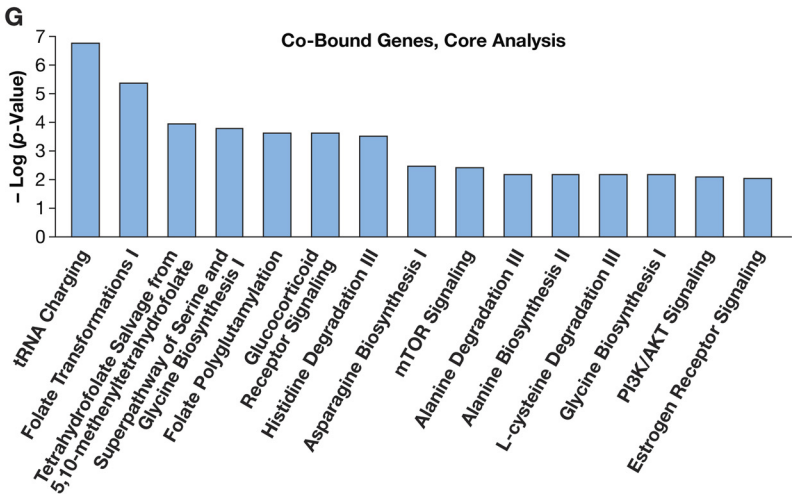

FIG 4 C/EBPγ and ATF4 coregulate many stress response genes and interact with common genomic targets. (A) Venn diagram showing overlap between C/EBPγ-dependent and ATF4-dependent genes induced by amino acid deprivation in MEFs. Of the 1,566 genes upregulated by AAD in WT MEFs, 248 were not induced in both *Cebpg*$^{-/-}$ and *Atf4*$^{-/-}$ cells. (B) Genome-wide (total) and transcription start site (TSS)-proximal ChIP-Seq peaks for ATF4, C/EBPγ, or both in MEFs exposed to AAD. (C) Venn diagram showing overlaps between the ATF4 and C/EBPγ TSS-proximal ChIP-Seq peaks and the 248 coregulated genes. (D) Clustering of C/EBPγ, ATF4, and cooccupied peaks immediately upstream of the TSS. TSS-proximal peak sets were used for the distance-to-TSS analysis. (E) Occurrence of CARE/AARE motifs in ATF4-bound and C/EBPγ-ATF4-cobound TSS-proximal peaks. (F) Sequence motifs associated with TSS-proximal ChIP-Seq peaks. Sequence logos generated by *de novo* motif analysis (occurrence in >50% of sequences) for ATF4 and cooccupied peaks are shown in alignment with the consensus CARE/AARE sequence. (G) Canonical pathways associated with the 83 genes displaying C/EBPγ and ATF4 cooccupancy in the TSS-proximal region. The top 15 pathways (Ingenuity Pathway Analysis) are shown.

Gross and detailed histologic analysis revealed that all newborn *Cebpg*$^{-/-}$ pups displayed atelectasis (lack of lung inflation) but no other obvious structural abnormalities (Fig. 9B). Thus, cause of death was interpreted to be respiratory failure secondary to impaired lung inflation. Examination of E18 *Cebpg*$^{-/-}$ embryos showed normal lung architecture (Fig. 9C), indicating that the respiratory defects of neonates are not developmental in origin.

Since treatment with NAC dramatically rescued the prolifera-

TABLE 1 Target genes coregulated by C/EBPγ and ATF4 are associated with stress responses, oxidative homeostasis, and lipid biosynthesis[a]

Gene	Description	Function[b]
A630007B06Rik/*Ccdc186*	Coiled-coil domain containing 186	Uncharacterized
Aars	Alanyl-tRNA synthetase	Catalyzes the attachment of alanine to tRNA (Ala); edits incorrectly charged tRNA (Ala)
Ankrd11	Ankyrin repeat domain 11	Inhibits ligand-dependent transcription activation
Arl14ep	ADP-ribosylation factor-like 14 effector protein	Connects MHC class II-containing cytoplasmic vesicles to the actin network and hence controls their export
Ddit4/REDD1	DNA damage-inducible transcript 4	Inhibits mTORC1 and participates in the cellular stress response
Gpt2	Glutamic pyruvate transaminase	Catalyzes the reversible transamination between alanine and 2-oxoglutarate to form pyruvate and glutamate
Herpud1	Homocysteine-inducible endoplasmic reticulum stress-inducible ubiquitin-like domain member	May play a role in UPR and ERAD; involved in ubiquitin-dependent degradation of misfolded ER proteins
Kdm6b/JMJD3	Lysine-specific demethylase 6b	Demethylates Lys-27 of histone H3
Pck2	Phosphoenolpyruvate carboxykinase 2	Catalyzes the conversion of oxaloacetate to phosphoenolpyruvate
Sesn2/HIF95	Sestrin2/hypoxia-induced gene 95	Plays a role in reducing peroxiredoxins
Slc7a11	Solute carrier family 7 (anionic amino acid transporter light chain, xc-system), member 11	Component of the amino acid transporter that exchanges anionic form of cysteine for glutamate
Soat2/ACACT2	**Sterol *O*-acyltransferase 2/acyl coenzyme A: cholesterol acyltransferase 2**	**Synthesizes cholesterol esters from long-chain fatty acyl coenzyme A and cholesterol**
Taf15	TATA box-binding protein-associated factor 2N	Subunit of transcription initiation complex
Trb3	Tribbles pseudokinase 3	Regulates ER stress; negatively regulates NF-κB and Akt1
Vldlr	**Very-low-density lipoprotein receptor**	**Mediates endocytosis of VLDL; stress induction of Nrf2 upregulates Vldlr**

[a] The table includes the 15 genes that are coregulated and cobound by C/EBPγ and ATF4 (Fig. 4D), along with descriptions of their functions. Shading indicates genes with known involvement in stress or oxidative homeostasis; boldface indicates genes associated with lipid metabolism/transport.
[b] MHC, major histocompatibility complex; ERAD, ER stress-associated protein degradation; VLDL, very-low-density lipoprotein; Vldlr, very-low-density lipoprotein receptor.

tion of *Cebpg*$^{-/-}$ MEFs, we hypothesized that sudden exposure to atmospheric oxygen might lead to oxidative lung damage in C/EBPγ-deficient pups. Therefore, we used NAC supplementation to determine if antioxidants could counteract possible oxidative stress in mutant lungs. NAC administration to pregnant mothers via chow and water significantly improved the viability of *Cebpg*$^{-/-}$ neonates (Fig. 9D). Of 10 mutant newborns born to NAC-treated mothers, three died on postnatal day 1 (P1), and the remainder survived for extended periods. Three mice were found cannibalized on P6 and P7, and their cause of death is unknown, but the remaining four mice were viable through weaning (Fig. 9D and E). This is a significant improvement compared to viability in

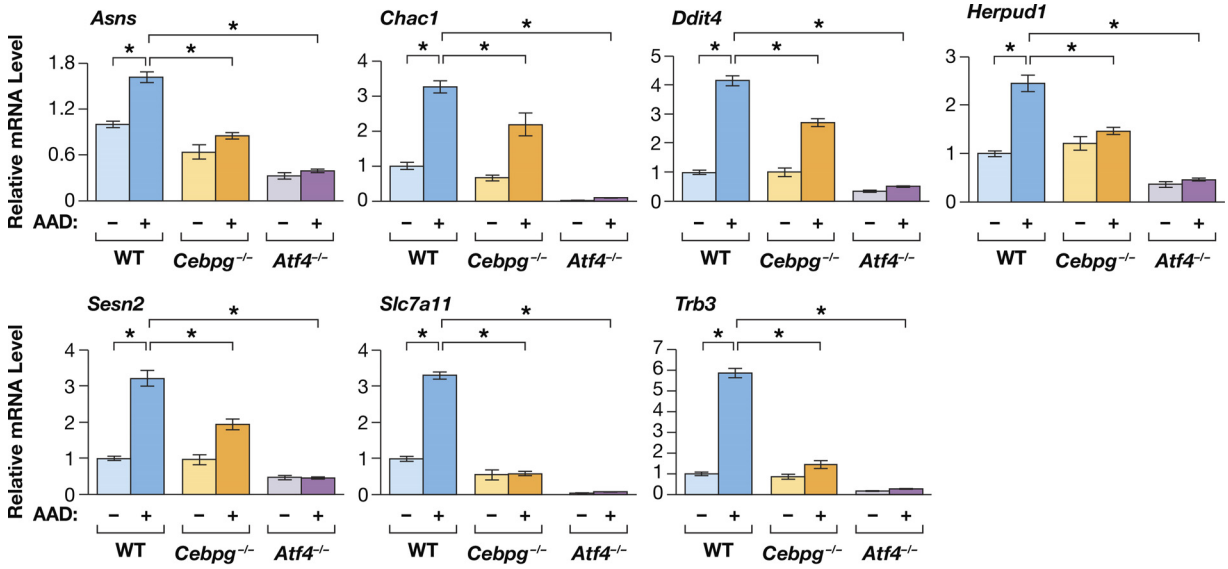

FIG 5 C/EBPγ and ATF4 are required for expression of stress-induced genes. Graphs show AAD-induced expression of stress response genes in WT, *Cebpg*$^{-/-}$, and *Atf4*$^{-/-}$ MEFs. mRNA levels were determined by qPCR. Data represent mean values ± SEM ($n = 2$). *, $P \leq 0.05$.

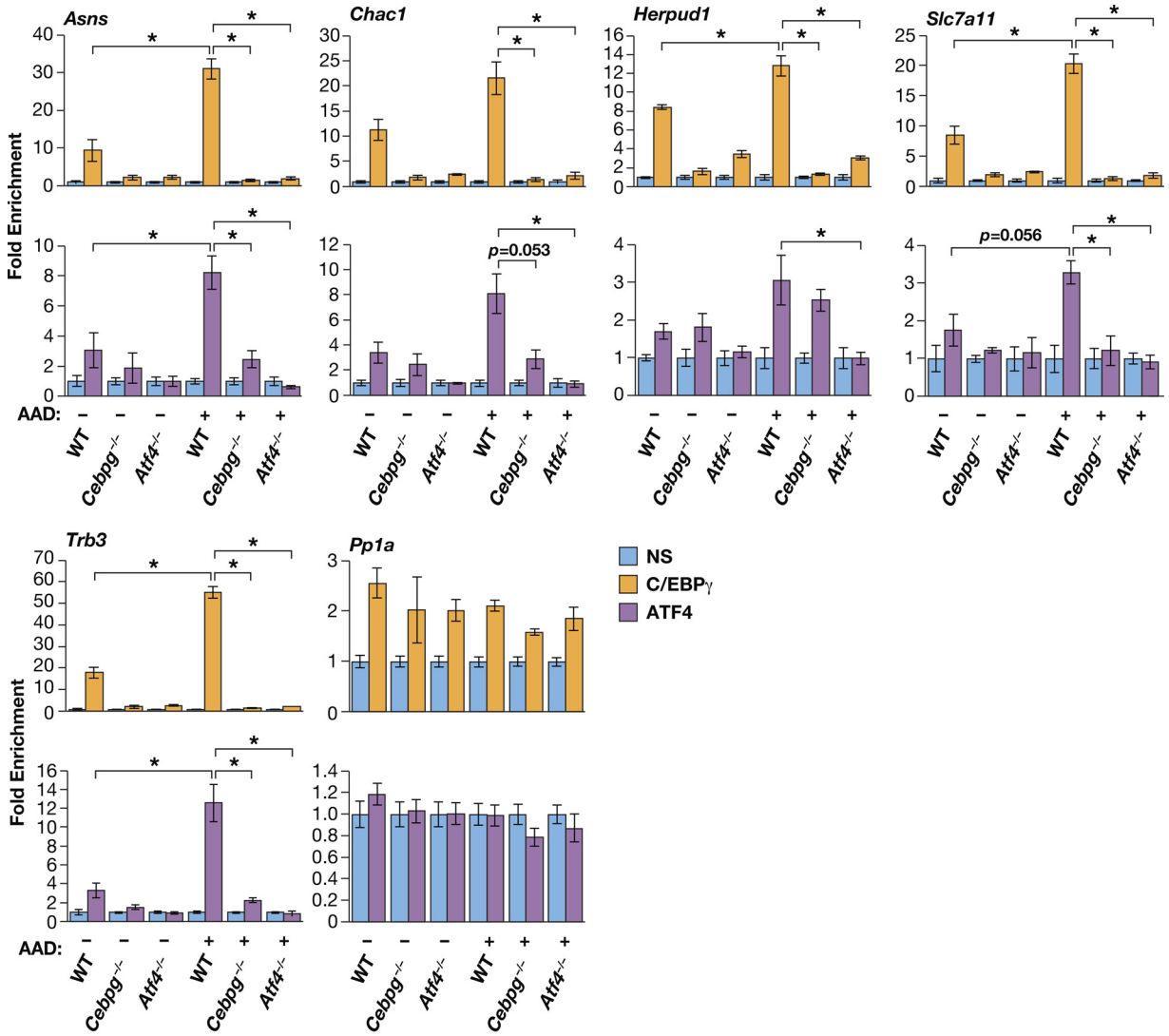

FIG 6 C/EBPγ and ATF4 bind in a mutually dependent manner to genomic CARE regions. Quantitative ChIP assays of AAD-induced C/EBPγ and ATF4 binding to CARE regions in stress-induced genes in WT, *Cebpg*$^{-/-}$, and *Atf4*$^{-/-}$ MEFs. *Pp1a* was included as a negative-control locus. Data are presented as mean values ± standard deviations ($n = 2$). *, $P \leq 0.05$.

untreated knockout (KO) pups, all six of which died on P1. Furthermore, *Cebpg*$^{-/-}$ neonates from NAC-treated mothers displayed greater lung inflation than their untreated counterparts (Fig. 9B versus F). Although the lungs of NAC-rescued mice did not show fully normal levels of expansion, their morphology was markedly improved relative to that of control *Cebpg*$^{-/-}$ animals.

Previous analysis of *Atf4*$^{-/-}$ mice showed that only ~40% of newborns survived through weaning (36, 37). Anemia was a major cause of death, with pale livers indicative of defective hematopoiesis (36, 38). We observed a sub-Mendelian ratio of newborn *Atf4*$^{-/-}$ mice (~30% less than predicted), yet most of the mutant neonates survived to weaning and beyond (Fig. 10A and data not shown). Accordingly, there was no discernible difference in the lungs of WT and *Atf4*$^{-/-}$ animals (Fig. 10B). Therefore, the early lethality of *Cebpg*$^{-/-}$ mice is not manifested in ATF4-deficient pups. Among their phenotypes, *Atf4*$^{-/-}$ pups exhibited reduced body size and abnormal eye lens development (37, 38) (Fig. 10C). The eye defect was also consistently observed in *Cebpg*$^{-/-}$ animals, which displayed small, deformed lenses that were vacuolized (Fig. 10C). Examination of *Cebpg*$^{-/-}$ E18 pups also revealed that lenses were incompletely formed (data not shown). This is consistent with observations for E14.5 *Atf4*$^{-/-}$ embryos, which at this stage of development show lens malformations involving p53-dependent apoptosis (38). Thus, both C/EBPγ and ATF4 are required for proper development of the lens, supporting the notion that they act as a heterodimer. In contrast to the rescue of atelectasis, NAC supplementation did not restore normal lens morphology in *Cebpg*$^{-/-}$ embryos (Fig. 10C).

Since *Atf4*$^{-/-}$ animals do not exhibit the atelectasis and perinatal lethality of *Cebpg*$^{-/-}$ mice, we considered that other ATF family members might heterodimerize with C/EBPγ to control antioxidant responses in the lung. ATF2 can be induced by stress and has been implicated in regulating oxidative homeostasis (39); like *Cebpg*$^{-/-}$ animals, *Atf2*$^{-/-}$ mice exhibit perinatal lethality due to severe respiratory distress (40). ATF2-deficient neonates contain meconium (fetal stool) in their lung alveolar spaces, a

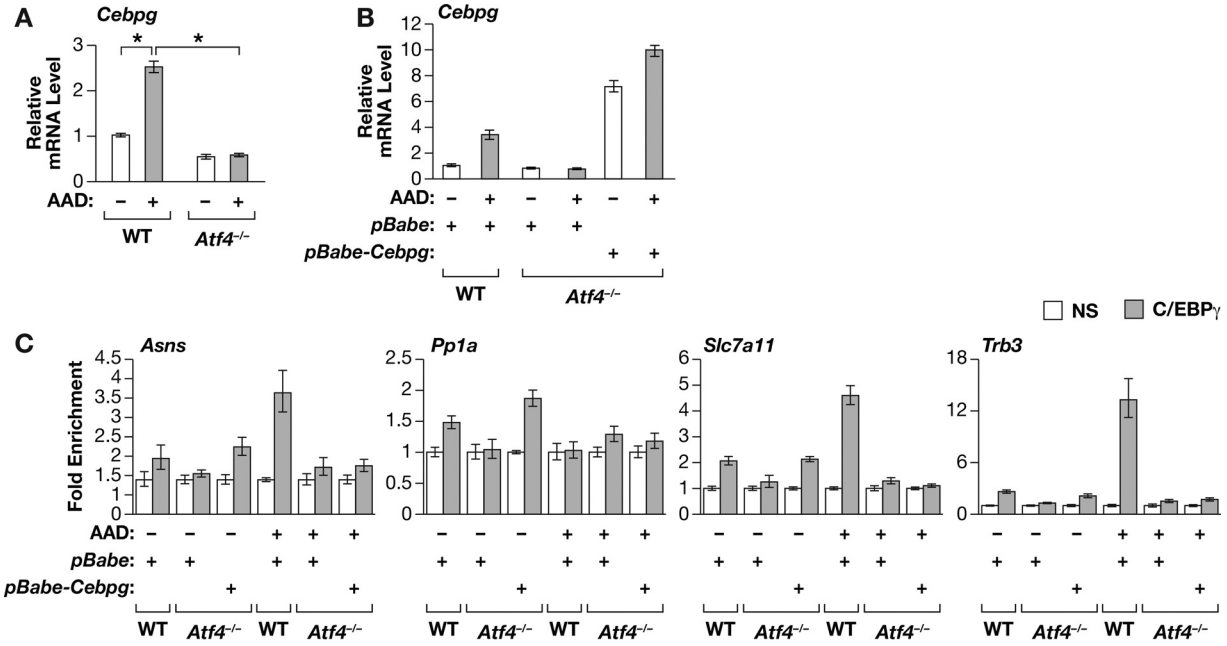

FIG 7 C/EBPγ is regulated by ATF4 at the mRNA level and requires ATF4 to bind to genomic targets. (A) Levels of *Cebpg* mRNA in WT and *Atf4*$^{-/-}$ MEFs in the absence or presence of stress (AAD), as measured by RT-qPCR. (B) Ectopic *Cebpg* mRNA expression in WT and *Atf4*$^{-/-}$ MEFs. Cells were infected with C/EBPγ-expressing or control pBabe vectors, and *Cebpg* mRNA levels were determined by RT-qPCR. (C) ChIP-qPCR assays of C/EBPγ binding to genomic CARE regions in WT and *Atf4*$^{-/-}$ MEFs, without or with C/EBPγ overexpression. Binding was analyzed in the absence or presence of stress (AAD). Data are presented as mean values ± standard deviations ($n = 1$, assayed in triplicate). *, $P \leq 0.05$.

consequence of gasping respiration and aspiration of amniotic fluid. This phenotype was proposed to arise from fetal hypoxia due to defective proliferation of embryo-derived cytotrophoblasts in the labyrinth layer of the placenta, causing insufficient oxygen exchange across the placental barrier (40). *Cebpg*$^{-/-}$ neonates similarly contained meconium in their lungs (Fig. 10D), suggesting a possible role for C/EBPγ:ATF2 heterodimers in lung and/or placenta. Accordingly, we detected a weakly expressed C/EBPγ:ATF2 heterodimeric CARE-binding complex in extracts from E18 lungs and placenta and in newborn lungs, but no evidence for an ATF4 DNA-binding species (Fig. 10E and F). Placentas from E18 *Cebpg*$^{-/-}$ embryos did not show morphological alterations in the labyrinth layer compared to the morphology of WT fetuses, and no decrease in cytotrophoblasts was observed (data not shown). Therefore, the respiratory defects in *Cebpg*$^{-/-}$ neonates may involve disregulation of C/EBPγ target genes in the lung and not the placenta.

mRNAs for *Ppargc1a* (PGC-1α) and *Cebpa*, lipogenic regulators that are induced by stress (41), were elevated in neonatal lungs of *Cebpg*$^{-/-}$ mice (Fig. 11A), indicating increased oxidative and/or ER stress. *Gpx4*, an Nrf2 target, was also induced in mutants, and all three genes were downregulated in NAC-treated animals (Fig. 11A). Genes involved in regeneration of GSH and oxidative homeostasis (*Gpx7* and *Mthfd2*) or regulation of stress responses (*Atf5*) showed significantly reduced expression in lungs of *Cebpg*$^{-/-}$ neonates versus that in WT mice (Fig. 10B). *Mthfd2* and *Atf5* were induced by AAD in WT MEFs but not in *Cebpg*$^{-/-}$ (or *Atf4*$^{-/-}$) cells (Fig. 11C), confirming their regulation by C/EBPγ. *Gpx7* levels were also downregulated in mutant cells, and C/EBPγ and ATF4 displayed mutually dependent binding to the CARE regions of *Mthfd2* and *Atf5* in stressed cells (Fig. 11D). These data suggest that impaired expression of antioxidant genes in C/EBPγ-deficient neonatal lung causes oxidative stress, leading to atelectasis.

Lung disfunction in *Cebpg*$^{-/-}$ mice could be caused by defects in the pulmonary surfactant lipoprotein complex, which is essential for proper lung expansion. Levels of several mRNAs involved in fatty acid synthesis (*Fasn*, *Soat1*, *Scd1*, *Elovl1*, and *LpCat1*) were decreased in mutant lung tissue, as was the level of surfactant protein C (Fig. 11E). Lipidomics analysis using mass spectrometry showed modest but significant reductions in total levels of several classes of surfactant lipids in *Cebpg*$^{-/-}$ lungs, including lysophosphatidylcholines, phosphatidylcholines, lysophosphatidyethanolamines, and phosphatidylethanolamines (Fig. 11F). Thus, impaired pulmonary surfactant homeostasis, possibly including oxidative damage to surfactant lipids, may explain the fatal respiratory distress syndrome in *Cebpg*$^{-/-}$ neonates.

Adult *Cebpg*$^{-/-}$ mice on a mixed strain background show increased early mortality and altered cancer incidence. We have observed that neonatal mortality of *Cebpg*$^{-/-}$ mice is diminished on a C57BL/6 × 129Sv (F1) mixed strain background (23), facilitating the analysis of adult mutant animals. Cohorts of viable WT and *Cebpg*$^{-/-}$ mice were used for aging studies to determine whether C/EBPγ deficiency affects life span and disease incidence. WT animals ($n = 148$) displayed a mean life span of 693 ± 115 days, while the average age of *Cebpg*$^{-/-}$ mice ($n = 52$) was lower (631 ± 231 days; $P = 0.025$). Kaplan-Meier survival curves showed that decreased viability of mutants occurs mainly in the shortest-lived 40% of animals (Fig. 12A, left panel), where the difference in mean ages of death between WT and mutants was especially pronounced (WT, 563 ± 115 days; *Cebpg*$^{-/-}$, 405 ± 214 days; $P = 0.00007$). This effect on mortality can be attributed

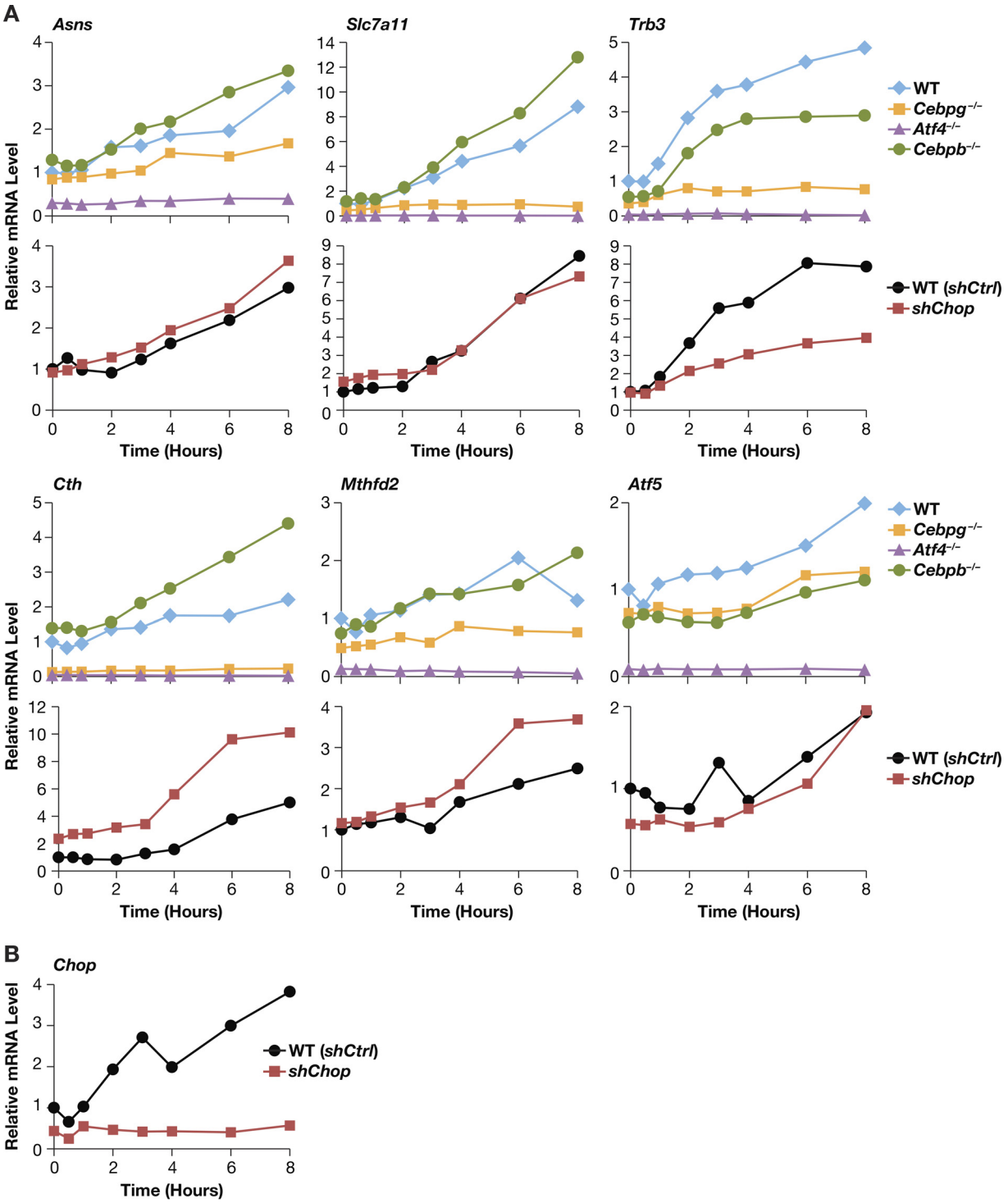

FIG 8 C/EBPβ and CHOP are largely dispensable for induction of ATF4-regulated stress genes in MEFs. (A) Each panel shows a time course of ATF4 target gene expression induced by AAD stress. The upper graphs depict mRNA levels for each gene in WT, *Cebpb*$^{-/-}$, *Cebpg*$^{-/-}$, and *Atf4*$^{-/-}$ MEFs; lower panels show the same genes in MEFs infected with an sh*Chop* or shCtrl knockdown vector. (B) Validation of *Chop* knockdown in MEFs.

to the female group; mutant males showed no differences in longevity (Fig. 12A, right panels).

Groups of WT and knockout animals were randomly selected for postmortem pathology evaluation (Fig. 12B; see also Tables S3 and S4 in the supplemental material). A notable difference was the reduced incidence of malignant solid (nonhematopoietic) tumors in *Cebpg*$^{-/-}$ mice compared to the incidence in WT animals (3% versus 18% of organs analyzed, respectively; $P = 0.0016$) (Fig. 12B; see also Table S4A in the supplemental material). Carcinomas of the liver and lung were the most prevalent cancers in WT

A

Genotype	Avg. Wt. at Birth (g)	No. Surviving Day 1	No. Surviving Day 2
Cebpg$^{+/+}$	1.35 ± 0.07	12/14 (85.7%)	11/14 (78.6%)
Cebpg$^{+/-}$	1.34 ± 0.10	29/34 (85.3%)	28/34 (82.3%)
Cebpg$^{-/-}$	1.22* ± 0.19	2/10 (20%)	0/10 (0%)

*p=0.02 (vs. +/+)

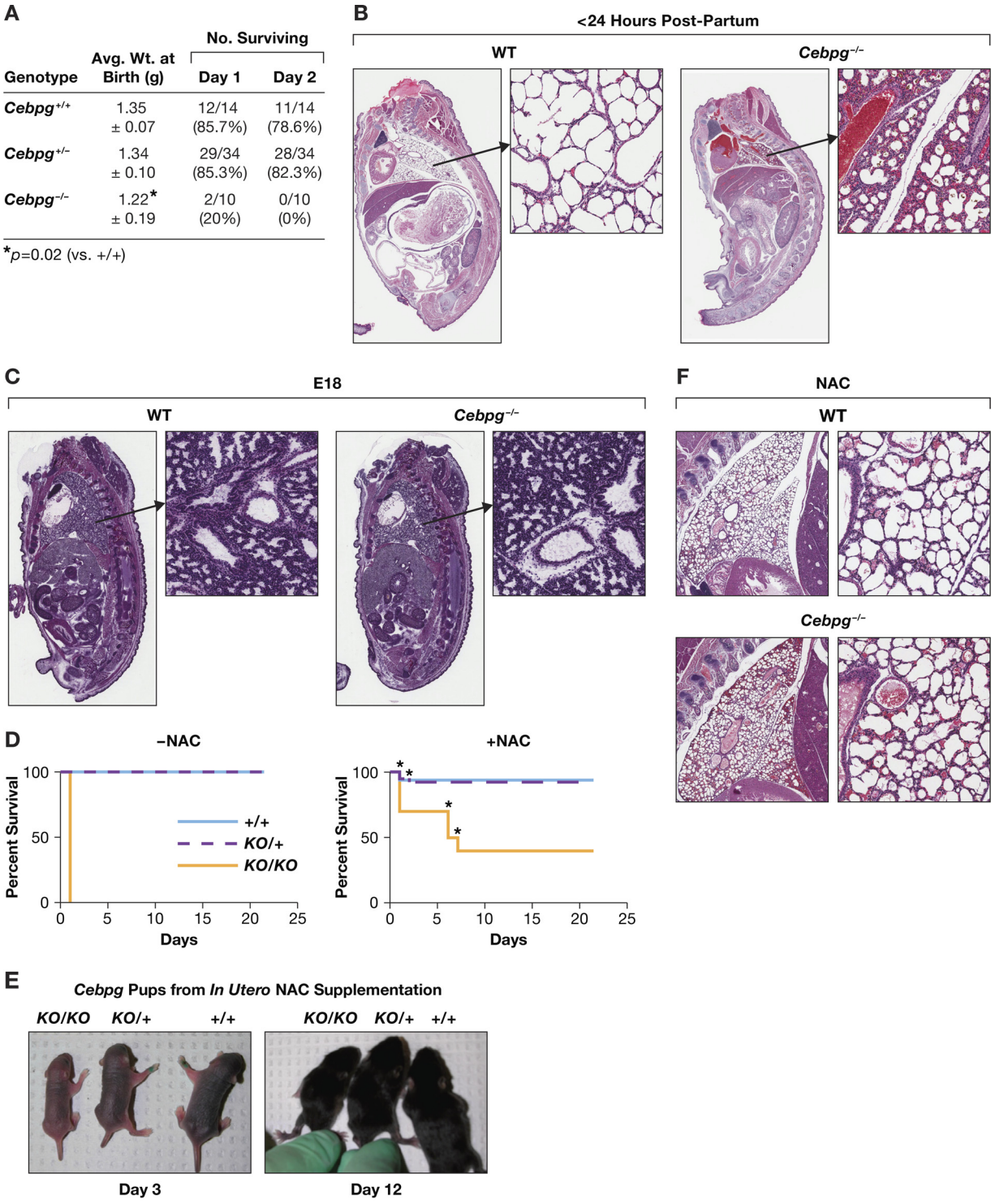

FIG 9 *Cebpg*$^{-/-}$ mice die perinatally from respiratory failure, which is substantially rescued by *in utero* exposure to NAC. (A) Birth weights and survival statistics for *Cebpg*$^{-/-}$ mice. (B) H&E-stained sections of WT and *Cebpg*$^{-/-}$ neonates. Whole-body images (×4 magnification; left panels) and magnified lungs (×20; right panels) reveal atelectasis in C/EBPγ-deficient animals. (C) Gross morphologies of WT and *Cebpg*$^{-/-}$ embryos (E18); whole-body images (×4 magnification; left panels) and magnified lungs (×20; right panels). The images are from frozen tissue sections. (D) Kaplan-Meier survival curves for WT, *Cebpg*$^{+/-}$, and *Cebpg*$^{-/-}$ newborn mice in the absence (−NAC) or presence (+NAC) of NAC *in utero*. Partial rescue of perinatal lethality is observed in the NAC-treated group. Asterisks indicate deaths from litters where the cause of death could not be determined due to cannibalization. (E) Photographs of littermates representing each of the three genotypes from NAC-treated mothers (days 3 and 12 postpartum). Note the smaller sizes of *Cebpg*$^{-/-}$ pups. (F) Lung sections (H&E staining) of WT and *Cebpg*$^{-/-}$ neonates (~48 h postpartum) treated with NAC *in utero*.

A

Genotype	Avg. Wt. at Birth (g)	No. Surviving Day 1	No. Surviving Day 2
Atf4$^{+/+}$	1.45±0.21	23/23 (100%)	23/23 (100%)
Atf4$^{+/-}$	1.51±0.25	42/42 (100%)	42/42 (100%)
Atf4$^{-/-}$	1.06*±0.14	14/14 (100%)	13/14 (92.8%)

*p=0.000014

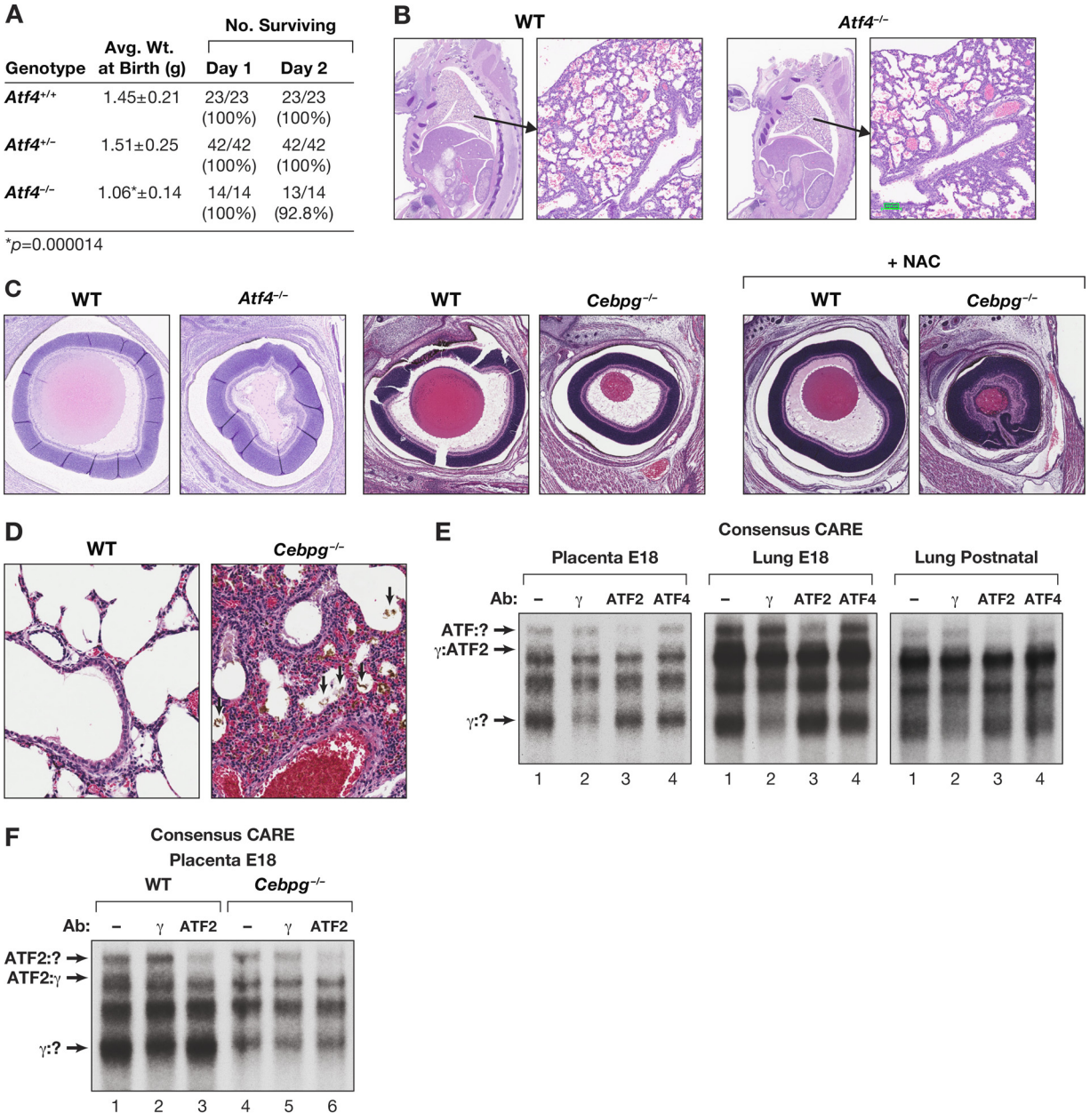

FIG 10 Comparative defects in fetal and neonatal *Cebpg*$^{-/-}$ and *Atf4*$^{-/-}$ mice. (A) Birth weights and survival statistics of *Atf4* mutant mice. (B) Gross morphologies of WT and *Atf4*$^{-/-}$ neonates. Whole-body images (×4 magnification; left panels) and magnified lungs (×20; right panels) are shown. (C) *Cebpg*$^{-/-}$ and *Atf4*$^{-/-}$ mice share similar eye lens defects. Images are from newborn animals. The *Cebpg*$^{-/-}$ lens phenotype is not rescued by *in utero* exposure to NAC (right panels). (D) Meconium is present in the lungs of newborn *Cebpg*$^{-/-}$ mice. Photomicrographs show meconium (arrows) in the alveolar spaces of *Cebpg*$^{-/-}$ pups, indicating gasping aspiration of amniotic fluid *in utero*. The phenotype is similar to that reported for *Atf2*$^{-/-}$ neonates (40). (E) Evidence for a CARE-binding ATF2:C/EBPγ heterodimer in the placenta and E18 and newborn lung tissues. EMSA was performed using nuclear extracts from the indicated tissues incubated with a consensus CARE probe. Supershift analysis was performed using C/EBPγ, ATF2, and ATF4 antibodies. Note the apparent absence of ATF4 complexes in all tissues. (F) Analysis of CARE-binding complexes in placental extracts from WT and *Cebpg*$^{-/-}$ embryos. Assays were performed without and with antibodies for C/EBPγ and ATF2. The mutant samples contain some C/EBPγ species derived from heterozygous maternal cells that contribute to the placenta.

mice but were rarely observed in mutant animals. However, there was no apparent difference in the incidence of benign tumors between the two genotypes (Fig. 12B; see also Table S4B in the supplemental material). These findings are consistent with the effects on tumorigenesis expected for animals with defective antioxidant and stress response pathways: namely, impaired development of malignant solid cancers that require efficient ROS suppression and alleviation of stress to facilitate growth and survival.

To extend these observations, we asked whether C/EBPγ regulates redox homeostasis in human cancer cells. Depletion of C/EBPγ in human A549 lung adenocarcinoma cells was previously shown to decrease proliferation and induce senescence

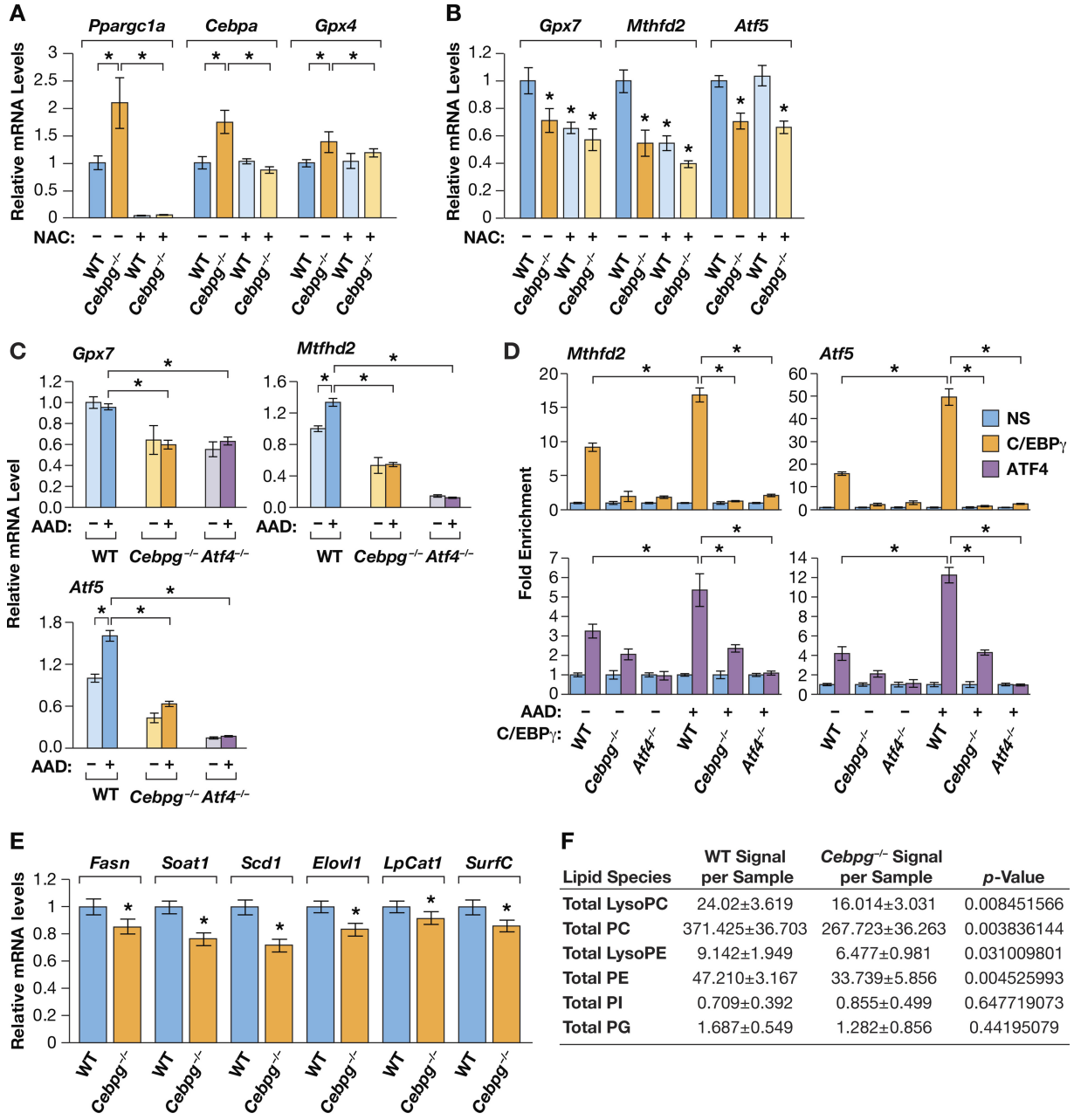

F

Lipid Species	WT Signal per Sample	*Cebpg*$^{-/-}$ Signal per Sample	*p*-Value
Total LysoPC	24.02±3.619	16.014±3.031	0.008451566
Total PC	371.425±36.703	267.723±36.263	0.003836144
Total LysoPE	9.142±1.949	6.477±0.981	0.031009801
Total PE	47.210±3.167	33.739±5.856	0.004525993
Total PI	0.709±0.392	0.855±0.499	0.647719073
Total PG	1.687±0.549	1.282±0.856	0.44195079

FIG 11 C/EBPγ regulates oxidative homeostasis in neonatal lung tissue. (A) mRNA levels of the oxidative stress markers *Ppargc1a*, *Cebpa*, and *Gpx4* in WT and *Cebpg*$^{-/-}$ neonatal lungs, with and without NAC supplementation during pregnancy. qPCR data represent mean values ± SEM ($n \geq 3$ for untreated animals; $n = 2$ for NAC-treated animals). (B) mRNA levels of genes involved in generating GSH (*Gpx7* and *Mthfd2*) and stress response regulation (*Atf5*) in lungs of WT and *Cebpg*$^{-/-}$ neonates, with and without NAC supplementation during pregnancy. qPCR data represent mean values ± SEM ($n \geq 3$ for untreated animals; $n = 2$ for NAC-treated animals). (C) C/EBPγ and ATF4 regulate stress-induced expression of *Gpx7*, *Mtfhd2*, and *Atf5* in MEFs. qPCR data are represented as mean values ± SEM ($n = 2$). (D) C/EBPγ and ATF4 bind in a mutually dependent manner to CARE regions in the *Mtfhd2* and *Atf5* promoters. *Gpx7* does not contain a recognizable CARE motif in the TSS-proximal region and was not included in this analysis. ChIP data are presented as mean values ± standard deviations ($n = 2$). (E) mRNA levels of genes associated with lipid biosynthesis and surfactant production in neonatal lung. Data are presented as mean values ± SEM ($n = 6$ for WT; $n = 5$ for *Cebpg*$^{-/-}$). (F) Analysis of surfactant phospholipids in lungs from WT and *Cebpg*$^{-/-}$ neonates ($n \geq 4$) as determined by mass spectrometry. Average levels of total lipid species per lung sample are shown. Lung weights were not statistically different between WT and mutant animals (data not shown). (Lyso)PC, (lyso)phosphatidylcholine; (Lyso)PE, (lyso)phosphatidylethanolamine; PI, phosphatidylinositol; PG, phosphatidylglycerol. *, $P \leq 0.05$.

(23). As shown in Fig. 12C, *CEBPG* knockdown suppressed A549 proliferation (colony formation), and this effect was substantially alleviated by NAC. The increase in senescent cells (SA-β-Gal staining) elicited by *CEBPG* depletion was also mitigated by NAC (Fig. 12D). Moreover, sh*CEBPG*-expressing A549 cells displayed a 6.5-fold increase in ROS levels, which was reversed by NAC treatment (Fig. 12E). Thus, C/EBPγ functions as a critical antioxidant regulator in human lung tumor cells, supporting the marked decrease in spontaneous lung tumors observed in *Cebpg*$^{-/-}$ mice.

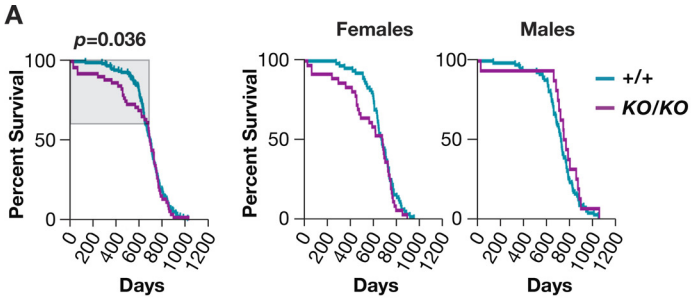

B

Type	Organ affected		Females WT (34)	Females *Cebpg*$^{-/-}$ (23)	Females p-value*	Males WT (37)	Males *Cebpg*$^{-/-}$ (15)	Males p-value*	All animals WT (71)	All animals *Cebpg*$^{-/-}$ (38)	All animals p-value*
Malignant (Non-Hematopoietic)	Heart, Liver, Lung, Skin/Subcutinis, Uterus	No. organs analyzed	73	52		67	21		140	73	
		No. malignant tumors	8	1		17	1		25	2	
		Incidence (%)	**10.96**	**1.92**	**0.0541**	**25.37**	**4.76**	**0.041**	**17.86**	**2.74**	**0.0016**
Benign	Duodenum, Harderian Gland, Kidney, Liver, Lung, Lymph node, Ovary, Pituitary, Skin/ Subcutinis, Uterus	No. organs analyzed	130	81		85	29		215	110	
		Benign tumors	14	5		12	8		26	13	
		Incidence (%)	**10.77**	**6.17**	**0.2567**	**14.12**	**27.59**	**0.0996**	**12.09**	**11.82**	**0.9425**

* Chi-Square Test

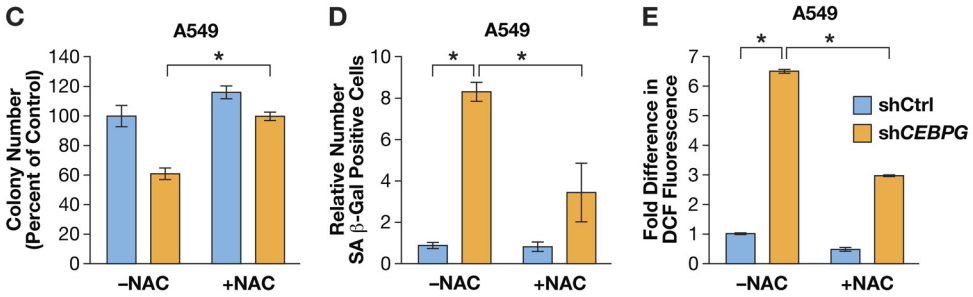

FIG 12 *Cebpg*$^{-/-}$ mice on a mixed (C57BL/6 × 129Sv) strain background survive at birth but display reduced viability in early adulthood and decreased incidence of malignant solid tumors. (A) Kaplan-Meier survival curves for WT and *Cebpg*$^{-/-}$ mice on a mixed strain background (C57BL/6 × 129Sv F1 hybrid). Animals genotyped at weaning (21 days) were used for the aging study. Data from all animals are shown in the left panel. A statistical comparison of the curves for the first 40% of aggregate life span (shaded box) shows increased early mortality for *Cebpg*$^{-/-}$ animals (Mantel-Cox log rank test). Survival data separated by gender are shown in the right panel. (B) Reduced incidence of malignant tumors in aged *Cebpg*$^{-/-}$ mice. Cancer data are from the subsets of WT and *Cebpg*$^{-/-}$ animals selected for pathology analysis in the aging study (see also Tables S3 and S4 in the supplemental material). (C to E) Human A549 lung adenocarcinoma cells require C/EBPγ for normal proliferation and oxidative homeostasis. Colony formation (C), senescence-associated β-galactosidase staining (D), and ROS levels (relative DCF fluorescence) (E) were analyzed in vector-infected and sh*CEBPG*-expressing cells. For ROS measurements, cells were grown in the absence and presence of NAC (1 mM). All data are presented as means ± SEM ($n = 2$). *, $P \leq 0.05$.

DISCUSSION

Cellular stresses typically induce the transcription factor ATF4, which activates genes that mitigate damage caused by oxidative stress, amino acid imbalances, or protein misfolding (13, 42–44). *Atf4*$^{-/-}$ MEFs exhibit impaired oxidative homeostasis due to reduced GSH pools and increased levels of ROS (1, 45). Here, we show that cells lacking C/EBPγ also display severe oxidative stress. These similarities arise from the fact that ATF4 preferentially heterodimerizes with C/EBPγ in stressed cells, forming a complex that is recruited to promoters with CARE/AARE motifs to activate expression of ISR genes. C/EBPγ is an essential partner of ATF4S as the two proteins act in a mutually dependent fashion to bind and activate stress response genes.

The identity of the C/EBP protein that dimerizes with ATF4 in stressed cells has been unclear, despite the well characterized role of CAREs in regulating ISR genes. Based on *in vitro* DNA-binding studies using recombinant proteins, C/EBPβ was proposed to interact with ATF4 at a CARE motif in the *cat-1* (*Slc7a1*) gene (14). However, we did not detect C/EBPβ:ATF4 heterodimers binding to CAREs *in vitro* using extracts from stressed MEF cells, and the induced CARE-binding complex was unaffected in C/EBPβ-deficient MEFs (Fig. 3). Although some stress genes are positively regulated by C/EBPβ, MEFs lacking C/EBPβ show normal or increased induction of several ISR genes (Fig. 8) (18). Thus, C/EBPβ may act primarily at later stages of the stress response by binding to CAREs and attenuating transcription (15, 18), possibly through expression of the inhibitory LIP isoform (46). Our results indicate that C/EBPγ is the predominant activator of ISR genes in fibroblasts and many tumor cells.

The notion that C/EBPγ is a critical ATF4 cofactor is further

supported by the shared phenotypes of mice lacking these proteins. *Cebpg*$^{-/-}$ and *Atf4*$^{-/-}$ animals both exhibit cataract-like lens malformations, indicating that the two genes function in a common pathway to regulate eye development (37). The similar microphthalmia phenotypes of *Cebpg*$^{-/-}$ and *Atf4*$^{-/-}$ mice may indicate coregulation of target genes by C/EBPγ:ATF4 heterodimers. Since differentiating fiber cells of the developing lens undergo a profound increase in membrane protein synthesis and display ER stress and activation of the UPR (38, 47), C/EBPγ:ATF4 dimers might regulate a protective gene expression program to maintain ER and oxidative homeostasis in these cells. Interestingly, we did not observe perinatal lethality and respiratory failure in ATF4 knockout mice although similar symptoms were reported for *Atf2*$^{-/-}$ animals (40). These respiratory phenotypes could be due to regulation of antioxidant genes by C/EBPγ:ATF2 heterodimers, a possibility supported by the detection of this CARE-binding complex in neonatal lung (Fig. 10E and F). These findings indicate that C/EBPγ can serve as a dimeric partner and regulatory cofactor for multiple ATF family members.

Several previous observations indicated the possibility of interactions between C/EBPγ and ATF4. ATF4 was identified in a phage screen for C/EBPγ-binding proteins (48), while C/EBPγ was selected as an ATF4 binding partner in a yeast two-hybrid screen using the ATF4 bZIP domain as bait (30). Studies using systematic peptide-based and *in silico* analyses of bZIP protein dimerization also suggested the potential for C/EBPγ:ATF4 interactions (17, 49, 50). Indeed, the C/EBPγ:ATF4 pair was one of the most avid and highly conserved leucine zipper associations identified in an evolutionary survey of bZIP protein:protein networks (49). These observations, together with our results, imply that the C/EBPγ:ATF4 dimer is an ancient adaptation that evolved in metazoans to regulate oxidative homeostasis and transcriptional responses to stress.

While C/EBPγ is a ubiquitously expressed protein (22, 51), its expression can be increased by stress. We observed a 2.5-fold induction of *Cebpg* mRNA by AAD in MEFs, possibly mediated by a CARE motif located in *Cebpg* intron 1 (GTTGCATCA) (see Table S2 in the supplemental material). *Cebpg* appeared as a stress-induced gene in several genome-wide expression studies (1, 52–55), and *CEBPG* mRNA levels were correlated with expression of antioxidant and DNA repair genes in human bronchial epithelial cells (56, 57). C/EBPγ may also have geno-protective functions as a consequence of its antioxidant activity. Interestingly, the naked mole rat (NMR), an exceptionally long-lived rodent used as a model of longevity (58), carries three copies of the *CEBPG* gene (59). Out of 518 genes implicated in genome maintenance, *CEBPG* and *TINF2* (involved in protecting telomere integrity) are the only two genes with increased copy numbers in the NMR genome compared to those in the mouse and human genomes. Therefore, *CEBPG* and *TINF2* were proposed to play roles in genome maintenance and life span extension. Our findings provide a plausible mechanism to connect increased *CEBPG* copy number with genome protection and longevity and possibly cancer resistance.

Our results have some intriguing parallels with recent observations on another C/EBP family member, CHOP (*Cebpz* or *Ddit3*). CHOP was found to interact with ATF4 to activate stress-induced genes that regulate protein synthesis, such as aminoacyl-tRNA synthetases (32, 44). We identified tRNA charging as the cellular process most highly correlated with genes cobound by C/EBPγ and ATF4 (Fig. 4G). Moreover, several tRNA synthetase genes (*Sars*, *Aars*, *Gars*, *Iars*, and *Yars*) displayed TSS-proximal C/EBPγ peaks associated with CAREs (see Table S1 in the supplemental material). Han et al. (32) reported that CHOP:ATF4 complexes also interact with genomic regions containing AARE/CAREs, presumably through direct binding to CARE motifs. However, while CHOP has a C/EBP-like leucine zipper, it lacks a characteristic bZIP basic region (60). Consequently, CHOP:C/EBPβ heterodimers recognize a unique sequence (61) that is different from the canonical palindromic motif bound by other C/EBP dimers (62). CHOP is therefore not expected to recognize the C/EBP half-site in CAREs, which should preclude CHOP:ATF4 dimers from binding to CAREs with high affinity. Accordingly, we did not detect a CHOP:ATF4 complex bound to CARE probes in EMSAs of stressed cells (data not shown); similar findings have been reported by others (63). It is possible that a unique CHOP:ATF4 binding site exists and that this element lies adjacent to CAREs in some stress-induced genes. In any case, C/EBPγ and CHOP do not display identical target gene specificities. For example, C/EBPγ and ATF4 activate genes involved in oxidative homeostasis and amino acid biosynthesis/transport (e.g., *Asns*, *Cth*, and *Herpud1*) that have not been linked to regulation by CHOP (1, 32).

The regulation of stress response genes is complex, and ATF4 partners can be influenced by the kind of stress and the cell type (13). CHOP has been shown to repress *Asns* expression via its CARE site upon ER stress or amino acid deprivation (30). On the other hand, CHOP induces *TRB3* upon ER stress, presumably through its association with CARE sites (64). Although there are common ATF4 transcriptional targets activated by a variety of stress signals, certain ATF4 targets are induced only in response to specific types of stress. The *SNAT2* gene is activated only by amino acid deprivation in human hepatoma cells even though ATF4 occupies the *SNAT2* CARE under both amino acid deprivation and ER stress (65). Whether C/EBPγ or C/EBPβ dimerizes with ATF4 can also vary depending on the context. For example, increased cellular confluence in human mesenchymal cells activates transcription of genes that convert mesenchymal cells to preadipocytes, and this is regulated by ATF4:C/EBPβ heterodimers bound to CARE sites in these genes (66). Detailed biochemical and molecular analyses are needed to clarify the common and unique roles of C/EBPγ, C/EBPβ, and CHOP in regulating stress response genes through association with ATF4 and to elucidate the molecular basis for their target specificities.

Recent studies have implicated C/EBPγ in promoting cancers such as acute myeloid leukemia (AML) and lung adenocarcinoma (23, 67), in accordance with the marked decrease in spontaneously arising malignant solid tumors we observed in *Cebpg*$^{-/-}$ mice (Fig. 12B). Our data provide a mechanistic basis for the prooncogenic functions of C/EBPγ, especially its ability to control antioxidant pathways crucial for the progression and metastasis of advanced cancers (6). For example, the C/EBPγ target gene *Slc7a11* (*xCT*) encodes a component of the cystine transporter complex that provides a source of cysteine for synthesis of glutathione and thioredoxin, two key antioxidants in tumor cells (8). The importance of *Slc7a11* in cancer is underscored by the observation that its expression is silenced by p53, and *Slc7a11* downregulation contributes to tumor suppression independently of p53's ability to elicit apoptosis and senescence (68). C/EBPγ may also support tumor cell growth and proliferation by promoting high rates of

protein synthesis and fatty acid/lipid biogenesis through upregulation of tRNA synthetases and genes such as *Soat2*, *Fasn*, *Scd1*, and *Vldlr*. We anticipate that additional analysis of C/EBPγ target genes will reveal further insights into the prooncogenic functions of this critical stress response regulator.

ACKNOWLEDGMENTS

We thank Tsuneyasu Kaisho for providing *Cebpg*$^{+/-}$ mice, Michael Kilberg for an ATF4 antibody, and Allen Kane (Scientific Publications, Graphics and Media, Leidos Biomedical Research, Inc., Frederick National Laboratory for Cancer Research) for preparation of figures.

This research was supported by the Intramural Research Program of the NIH, National Cancer Institute, Center for Cancer Research, and in part with federal funds from the National Cancer Institute, National Institutes of Health, under contract number HHSN261200800001E.

The content of this publication does not necessarily reflect the views or policies of the Department of Health and Human Services, nor does mention of trade names, commercial products, or organizations imply endorsement by the U.S. Government.

FUNDING INFORMATION

HHS | NIH | National Cancer Institute (NCI) provided funding to Christopher J. Huggins, Manasi K. Mayekar, Nancy Martin, Karen L. Saylor, Mesfin Gonit, Parthav Jailwala, Manjula Kasoji, Diana C. Haines, Octavio A. Quinones, and Peter F. Johnson. HHS | NIH | National Cancer Institute (NCI) provided funding to Diana C. Haines under grant number contract no. HHSN261200800001E.

REFERENCES

1. **Harding HP, Zhang Y, Zeng H, Novoa I, Lu PD, Calfon M, Sadri N, Yun C, Popko B, Paules R, Stojdl DF, Bell JC, Hettmann T, Leiden JM, Ron D.** 2003. An integrated stress response regulates amino acid metabolism and resistance to oxidative stress. Mol Cell **11:**619–633. http://dx.doi.org/10.1016/S1097-2765(03)00105-9.
2. **Zinszner H, Kuroda M, Wang X, Batchvarova N, Lightfoot RT, Remotti H, Stevens JL, Ron D.** 1998. CHOP is implicated in programmed cell death in response to impaired function of the endoplasmic reticulum. Genes Dev **12:**982–995. http://dx.doi.org/10.1101/gad.12.7.982.
3. **Wang S, Kaufman RJ.** 2012. The impact of the unfolded protein response on human disease. J Cell Biol **197:**857–867. http://dx.doi.org/10.1083/jcb.201110131.
4. **Singleton DC, Harris AL.** 2012. Targeting the ATF4 pathway in cancer therapy. Expert Opin Ther Targets **16:**1189–1202. http://dx.doi.org/10.1517/14728222.2012.728207.
5. **Ye J, Kumanova M, Hart LS, Sloane K, Zhang H, De Panis DN, Bobrovnikova-Marjon E, Diehl JA, Ron D, Koumenis C.** 2010. The GCN2-ATF4 pathway is critical for tumour cell survival and proliferation in response to nutrient deprivation. EMBO J **29:**2082–2096. http://dx.doi.org/10.1038/emboj.2010.81.
6. **Gorrini C, Harris IS, Mak TW.** 2013. Modulation of oxidative stress as an anticancer strategy. Nat Rev Drug Discov **12:**931–947. http://dx.doi.org/10.1038/nrd4002.
7. **Sayin VI, Ibrahim MX, Larsson E, Nilsson JA, Lindahl P, Bergo MO.** 2014. Antioxidants accelerate lung cancer progression in mice. Sci Transl Med **6:**221ra15. http://dx.doi.org/10.1126/scitranslmed.3007653.
8. **Harris IS, Treloar AE, Inoue S, Sasaki M, Gorrini C, Lee KC, Yung KY, Brenner D, Knobbe-Thomsen CB, Cox MA, Elia A, Berger T, Cescon DW, Adeoye A, Brustle A, Molyneux SD, Mason JM, Li WY, Yamamoto K, Wakeham A, Berman HK, Khokha R, Done SJ, Kavanagh TJ, Lam CW, Mak TW.** 2015. Glutathione and thioredoxin antioxidant pathways synergize to drive cancer initiation and progression. Cancer Cell **27:**211–222. http://dx.doi.org/10.1016/j.ccell.2014.11.019.
9. **Ron D, Harding HP.** 2012. Protein-folding homeostasis in the endoplasmic reticulum and nutritional regulation. Cold Spring Harb Perspect Biol **4:**a013177. http://dx.doi.org/10.1101/cshperspect.a013177.
10. **Rutkowski DT, Kaufman RJ.** 2003. All roads lead to ATF4. Dev Cell **4:**442–444. http://dx.doi.org/10.1016/S1534-5807(03)00100-X.
11. **Tabas I, Ron D.** 2011. Integrating the mechanisms of apoptosis induced by endoplasmic reticulum stress. Nat Cell Biol **13:**184–190. http://dx.doi.org/10.1038/ncb0311-184.
12. **Kilberg MS, Shan J, Su N.** 2009. ATF4-dependent transcription mediates signaling of amino acid limitation. Trends Endocrinol Metab **20:**436–443. http://dx.doi.org/10.1016/j.tem.2009.05.008.
13. **Kilberg MS, Balasubramanian M, Fu L, Shan J.** 2012. The transcription factor network associated with the amino acid response in mammalian cells. Adv Nutr **3:**295–306. http://dx.doi.org/10.3945/an.112.001891.
14. **Lopez AB, Wang C, Huang CC, Yaman I, Li Y, Chakravarty K, Johnson PF, Chiang CM, Snider MD, Wek RC, Hatzoglou M.** 2007. A feedback transcriptional mechanism controls the level of the arginine/lysine transporter cat-1 during amino acid starvation. Biochem J **402:**163–173. http://dx.doi.org/10.1042/BJ20060941.
15. **Thiaville MM, Dudenhausen EE, Zhong C, Pan YX, Kilberg MS.** 2008. Deprivation of protein or amino acid induces C/EBPβ synthesis and binding to amino acid response elements, but its action is not an absolute requirement for enhanced transcription. Biochem J **410:**473–484. http://dx.doi.org/10.1042/BJ20071252.
16. **Mann IK, Chatterjee R, Zhao J, He X, Weirauch MT, Hughes TR, Vinson C.** 2013. CG methylated microarrays identify a novel methylated sequence bound by the CEBPB|ATF4 heterodimer that is active in vivo. Genome Res **23:**988–997. http://dx.doi.org/10.1101/gr.146654.112.
17. **Newman JR, Keating AE.** 2003. Comprehensive identification of human bZIP interactions with coiled-coil arrays. Science **300:**2097–2101. http://dx.doi.org/10.1126/science.1084648.
18. **Li Y, Bevilacqua E, Chiribau CB, Majumder M, Wang C, Croniger CM, Snider MD, Johnson PF, Hatzoglou M.** 2008. Differential control of the CCAAT/enhancer-binding protein beta (C/EBPβ) products liver-enriched transcriptional activating protein (LAP) and liver-enriched transcriptional inhibitory protein (LIP) and the regulation of gene expression during the response to endoplasmic reticulum stress. J Biol Chem **283:**22443–22456. http://dx.doi.org/10.1074/jbc.M801046200.
19. **Cooper C, Henderson A, Artandi S, Avitahl N, Calame K.** 1995. Ig/EBP (C/EBPγ) is a transdominant negative inhibitor of C/EBP family transcriptional activators. Nucleic Acids Res **23:**4371–4377. http://dx.doi.org/10.1093/nar/23.21.4371.
20. **Thomassin H, Hamel D, Bernier D, Guertin M, Belanger L.** 1992. Molecular cloning of two C/EBP-related proteins that bind to the promoter and the enhancer of the alpha 1-fetoprotein gene. Further analysis of C/EBPβ and C/EBPγ. Nucleic Acids Res **20:**3091–3098.
21. **Hattori T, Ohoka N, Inoue Y, Hayashi H, Onozaki K.** 2003. C/EBP family transcription factors are degraded by the proteasome but stabilized by forming dimer. Oncogene **22:**1273–1280. http://dx.doi.org/10.1038/sj.onc.1206204.
22. **Parkin SE, Baer M, Copeland TD, Schwartz RC, Johnson PF.** 2002. Regulation of CCAAT/enhancer-binding protein (C/EBP) activator proteins by heterodimerization with C/EBPγ (Ig/EBP). J Biol Chem **277:**23563–23572. http://dx.doi.org/10.1074/jbc.M202184200.
23. **Huggins CJ, Malik R, Lee S, Salotti J, Thomas S, Martin N, Quinones OA, Alvord WG, Olanich ME, Keller JR, Johnson PF.** 2013. C/EBPγ suppresses senescence and inflammatory gene expression by heterodimerizing with C/EBPβ. Mol Cell Biol **33:**3242–3258. http://dx.doi.org/10.1128/MCB.01674-12.
24. **Kaisho T, Tsutsui H, Tanaka T, Tsujimura T, Takeda K, Kawai T, Yoshida N, Nakanishi K, Akira S.** 1999. Impairment of natural killer cytotoxic activity and interferon gamma production in CCAAT/enhancer binding protein gamma-deficient mice. J Exp Med **190:**1573–1582. http://dx.doi.org/10.1084/jem.190.11.1573.
25. **Sterneck E, Tessarollo L, Johnson PF.** 1997. An essential role for C/EBPβ in female reproduction. Genes Dev **11:**2153–2162. http://dx.doi.org/10.1101/gad.11.17.2153.
26. **Sebastian T, Malik R, Thomas S, Sage J, Johnson PF.** 2005. C/EBPβ cooperates with RB:E2F to implement Ras^{V12}-induced cellular senescence. EMBO J **24:**3301–3312. http://dx.doi.org/10.1038/sj.emboj.7600789.
27. **National Research Council.** 1996. Guide for the care and use of laboratory animals. National Academy Press, Washington, DC.
28. **Baer M, Johnson PF.** 2000. Generation of truncated C/EBPβ isoforms by in vitro proteolysis. J Biol Chem **275:**26582–26590. http://dx.doi.org/10.1074/jbc.M004268200.
29. **Basu SK, Malik R, Huggins CJ, Lee S, Sebastian T, Sakchaisri K, Quinones OA, Alvord WG, Johnson PF.** 2011. 3′ UTR elements inhibit Ras-induced C/EBPβ post-translational activation and senescence in tu-

mour cells. EMBO J **30:**3714–3728. http://dx.doi.org/10.1038/emboj.2011.250.
30. **Su N, Kilberg MS.** 2008. C/EBP homology protein (CHOP) interacts with activating transcription factor 4 (ATF4) and negatively regulates the stress-dependent induction of the asparagine synthetase gene. J Biol Chem **283:**35106–35117. http://dx.doi.org/10.1074/jbc.M806874200.
31. **Krylov D, Mikhailenko I, Vinson C.** 1994. A thermodynamic scale for leucine zipper stability and dimerization specificity: e and g interhelical interactions. EMBO J **13:**2849–2861.
32. **Han J, Back SH, Hur J, Lin YH, Gildersleeve R, Shan J, Yuan CL, Krokowski D, Wang S, Hatzoglou M, Kilberg MS, Sartor MA, Kaufman RJ.** 2013. ER-stress-induced transcriptional regulation increases protein synthesis leading to cell death. Nat Cell Biol **15:**481–490. http://dx.doi.org/10.1038/ncb2738.
33. **Joshi R, Adhikari S, Patro BS, Chattopadhyay S, Mukherjee T.** 2001. Free radical scavenging behavior of folic acid: evidence for possible antioxidant activity. Free Radic Biol Med **30:**1390–1399. http://dx.doi.org/10.1016/S0891-5849(01)00543-3.
34. **Huang RF, Yaong HC, Chen SC, Lu YF.** 2004. In vitro folate supplementation alleviates oxidative stress, mitochondria-associated death signalling and apoptosis induced by 7-ketocholesterol. Br J Nutr **92:**887–894. http://dx.doi.org/10.1079/BJN20041259.
35. **Basseri S, and Austin RC.**2012. Endoplasmic reticulum stress and lipid metabolism: mechanisms and therapeutic potential. Biochem Res Int **2012:**841362. http://dx.doi.org/10.1155/2012/841362.
36. **Masuoka HC, Townes TM.** 2002. Targeted disruption of the activating transcription factor 4 gene results in severe fetal anemia in mice. Blood **99:**736–745. http://dx.doi.org/10.1182/blood.V99.3.736.
37. **Tanaka T, Tsujimura T, Takeda K, Sugihara A, Maekawa A, Terada N, Yoshida N, Akira S.** 1998. Targeted disruption of ATF4 discloses its essential role in the formation of eye lens fibres. Genes Cells **3:**801–810. http://dx.doi.org/10.1046/j.1365-2443.1998.00230.x.
38. **Hettmann T, Barton K, Leiden JM.** 2000. Microphthalmia due to p53-mediated apoptosis of anterior lens epithelial cells in mice lacking the CREB-2 transcription factor. Dev Biol **222:**110–123. http://dx.doi.org/10.1006/dbio.2000.9699.
39. **Walluscheck D, Poehlmann A, Hartig R, Lendeckel U, Schonfeld P, Hotz-Wagenblatt A, Reissig K, Bajbouj K, Roessner A, Schneider-Stock R.** 2013. ATF2 knockdown reinforces oxidative stress-induced apoptosis in TE7 cancer cells. J Cell Mol Med **17:**976–988. http://dx.doi.org/10.1111/jcmm.12071.
40. **Maekawa T, Bernier F, Sato M, Nomura S, Singh M, Inoue Y, Tokunaga T, Imai H, Yokoyama M, Reimold A, Glimcher LH, Ishii S.** 1999. Mouse ATF-2 null mutants display features of a severe type of meconium aspiration syndrome. J Biol Chem **274:**17813–17819. http://dx.doi.org/10.1074/jbc.274.25.17813.
41. **Lee JS, Mendez R, Heng HH, Yang ZQ, Zhang K.** 2012. Pharmacological ER stress promotes hepatic lipogenesis and lipid droplet formation. Am J Transl Res **4:**102–113.
42. **Hetz C.** 2012. The unfolded protein response: controlling cell fate decisions under ER stress and beyond. Nat Rev Mol Cell Biol **13:**89–102. http://dx.doi.org/10.1038/nrm3270.
43. **Walter P, Ron D.** 2011. The unfolded protein response: from stress pathway to homeostatic regulation. Science **334:**1081–1086. http://dx.doi.org/10.1126/science.1209038.
44. **Krokowski D, Han J, Saikia M, Majumder M, Yuan CL, Guan BJ, Bevilacqua E, Bussolati O, Broer S, Arvan P, Tchorzewski M, Snider MD, Puchowicz M, Croniger CM, Kimball SR, Pan T, Koromilas AE, Kaufman RJ, Hatzoglou M.** 2013. A self-defeating anabolic program leads to beta-cell apoptosis in endoplasmic reticulum stress-induced diabetes via regulation of amino acid flux. J Biol Chem **288:**17202–17213. http://dx.doi.org/10.1074/jbc.M113.466920.
45. **Dickhout JG, Carlisle RE, Jerome DE, Mohammed-Ali Z, Jiang H, Yang G, Mani S, Garg SK, Banerjee R, Kaufman RJ, Maclean KN, Wang R, Austin RC.** 2012. Integrated stress response modulates cellular redox state via induction of cystathionine gamma-lyase: cross-talk between integrated stress response and thiol metabolism. J Biol Chem **287:**7603–7614. http://dx.doi.org/10.1074/jbc.M111.304576.
46. **Descombes P, Schibler U.** 1991. A liver-enriched transcriptional activator protein, LAP, and a transcriptional inhibitory protein, LIP, are translated from the same mRNA. Cell **67:**569–579. http://dx.doi.org/10.1016/0092-8674(91)90531-3.
47. **Firtina Z, Duncan MK.** 2011. Unfolded protein response (UPR) is activated during normal lens development. Gene Expr Patterns **11:**135–143. http://dx.doi.org/10.1016/j.gep.2010.10.005.
48. **Nishizawa M, Wakabayashi-Ito N, Nagata S.** 1991. Molecular cloning of cDNA and a chromosomal gene encoding GPE1-BP, a nuclear protein which binds to granulocyte colony-stimulating factor promoter element 1. FEBS Lett **282:**95–97. http://dx.doi.org/10.1016/0014-5793(91)80452-9.
49. **Reinke AW, Baek J, Ashenberg O, Keating AE.** 2013. Networks of bZIP protein-protein interactions diversified over a billion years of evolution. Science **340:**730–734. http://dx.doi.org/10.1126/science.1233465.
50. **Grigoryan G, Reinke AW, Keating AE.** 2009. Design of protein-interaction specificity gives selective bZIP-binding peptides. Nature **458:**859–864. http://dx.doi.org/10.1038/nature07885.
51. **Roman C, Platero JS, Shuman J, Calame K.** 1990. Ig/EBP-1: a ubiquitously expressed immunoglobulin enhancer binding protein that is similar to C/EBP and heterodimerizes with C/EBP. Genes Dev **4:**1404–1415. http://dx.doi.org/10.1101/gad.4.8.1404.
52. **Lee JI, Dominy JE, Jr, Sikalidis AK, Hirschberger LL, Wang W, Stipanuk MH.** 2008. HepG2/C3A cells respond to cysteine deprivation by induction of the amino acid deprivation/integrated stress response pathway. Physiol Genomics **33:**218–229. http://dx.doi.org/10.1152/physiolgenomics.00263.2007.
53. **Lu PD, Jousse C, Marciniak SJ, Zhang Y, Novoa I, Scheuner D, Kaufman RJ, Ron D, Harding HP.** 2004. Cytoprotection by pre-emptive conditional phosphorylation of translation initiation factor 2. EMBO J **23:**169–179. http://dx.doi.org/10.1038/sj.emboj.7600030.
54. **Rutkowski DT, Wu J, Back SH, Callaghan MU, Ferris SP, Iqbal J, Clark R, Miao H, Hassler JR, Fornek J, Katze MG, Hussain MM, Song B, Swathirajan J, Wang J, Yau GD, Kaufman RJ.** 2008. UPR pathways combine to prevent hepatic steatosis caused by ER stress-mediated suppression of transcriptional master regulators. Dev Cell **15:**829–840. http://dx.doi.org/10.1016/j.devcel.2008.10.015.
55. **Sikalidis AK, Lee JI, Stipanuk MH.** 2011. Gene expression and integrated stress response in HepG2/C3A cells cultured in amino acid deficient medium. Amino Acids **41:**159–171. http://dx.doi.org/10.1007/s00726-010-0571-x.
56. **Mullins DN, Crawford EL, Khuder SA, Hernandez DA, Yoon Y, Willey JC.** 2005. CEBPG transcription factor correlates with antioxidant and DNA repair genes in normal bronchial epithelial cells but not in individuals with bronchogenic carcinoma. BMC Cancer **5:**141. http://dx.doi.org/10.1186/1471-2407-5-141.
57. **Crawford EL, Blomquist T, Mullins DN, Yoon Y, Hernandez DR, Al-Bagdhadi M, Ruiz J, Hammersley J, Willey JC.** 2007. CEBPG regulates ERCC5/XPG expression in human bronchial epithelial cells and this regulation is modified by E2F1/YY1 interactions. Carcinogenesis **28:**2552–2559. http://dx.doi.org/10.1093/carcin/bgm214.
58. **Gorbunova V, Seluanov A, Zhang Z, Gladyshev VN, Vijg J.** 2014. Comparative genetics of longevity and cancer: insights from long-lived rodents. Nat Rev Genet **15:**531–540. http://dx.doi.org/10.1038/nrg3728.
59. **MacRae SL, Zhang Q, Lemetre C, Seim I, Calder RB, Hoeijmakers J, Suh Y, Gladyshev VN, Seluanov A, Gorbunova V, Vijg J, Zhang ZD.** 2015. Comparative analysis of genome maintenance genes in naked mole rat, mouse, and human. Aging Cell **14:**288–291. http://dx.doi.org/10.1111/acel.12314.
60. **Ron D, Habener JF.** 1992. CHOP, a novel developmentally regulated nuclear protein that dimerizes with transcription factors C/EBP and LAP and functions as a dominant-negative inhibitor of gene transcription. Genes Dev **6:**439–453. http://dx.doi.org/10.1101/gad.6.3.439.
61. **Ubeda M, Wang XZ, Zinszner H, Wu I, Habener JF, Ron D.** 1996. Stress-induced binding of the transcriptional factor CHOP to a novel DNA control element. Mol Cell Biol **16:**1479–1489. http://dx.doi.org/10.1128/MCB.16.4.1479.
62. **Johnson PF.** 1993. Identification of C/EBP basic region residues involved in DNA sequence recognition and half-site spacing preference. Mol Cell Biol **13:**6919–6930. http://dx.doi.org/10.1128/MCB.13.11.6919.
63. **Jiang HY, Wek SA, McGrath BC, Lu D, Hai T, Harding HP, Wang X, Ron D, Cavener DR, Wek RC.** 2004. Activating transcription factor 3 is integral to the eukaryotic initiation factor 2 kinase stress response. Mol Cell Biol **24:**1365–1377. http://dx.doi.org/10.1128/MCB.24.3.1365-1377.2004.
64. **Ohoka N, Yoshii S, Hattori T, Onozaki K, Hayashi H.** 2005. TRB3, a novel ER stress-inducible gene, is induced via ATF4-CHOP pathway and is involved in cell death. EMBO J **24:**1243–1255. http://dx.doi.org/10.1038/sj.emboj.7600596.

65. **Gjymishka A, Palii SS, Shan J, Kilberg MS.** 2008. Despite increased ATF4 binding at the C/EBP-ATF composite site following activation of the unfolded protein response, system A transporter 2 (SNAT2) transcription activity is repressed in HepG2 cells. J Biol Chem **283:**27736–27747. http://dx.doi.org/10.1074/jbc.M803781200.
66. **Cohen DM, Won KJ, Nguyen N, Lazar MA, Chen CS, Steger DJ.** 2015. ATF4 licenses C/EBPβ activity in human mesenchymal stem cells primed for adipogenesis. eLife **4:**e06821. http://dx.doi.org/10.7554/eLife.06821.
67. **Alberich-Jorda M, Wouters B, Balastik M, Shapiro-Koss C, Zhang H, Di Ruscio A, Radomska HS, Ebralidze AK, Amabile G, Ye M, Zhang J, Lowers I, Avellino R, Melnick A, Figueroa ME, Valk PJ, Delwel R, Tenen DG.** 2013. C/EBPγ deregulation results in differentiation arrest in acute myeloid leukemia. J Clin Invest **122:**4490–4504. http://dx.doi.org/10.1172/JCI65102.
68. **Jiang L, Kon N, Li T, Wang SJ, Su T, Hibshoosh H, Baer R, Gu W.** 2015. Ferroptosis as a p53-mediated activity during tumour suppression. Nature **520:**57–62. http://dx.doi.org/10.1038/nature14344.